

Potential of Multimodal Large Language Models for Data Mining of Medical Images and Free-text Reports

Yutong Zhang ^{*1}, Yi Pan ^{*2,3}, Tianyang Zhong ^{*4}, Peixin Dong ^{†4}, Kangni Xie ^{†5}, Yuxiao Liu ^{†6,7}, Hanqi Jiang², Zhengliang Liu², Shijie Zhao⁴, Tuo Zhang⁴, Xi Jiang³, Dinggang Shen^{6,8,9}, Tianming Liu², and Xin Zhang^{‡1}

¹Institute of Medical Research, Northwestern Polytechnical University, Xi'an 710072, China

²School of Computing, University of Georgia, GA, USA

³School of Life Science and Technology, University of Electronic Science and Technology of China, Chengdu 611731, China

⁴School of Automation, Northwestern Polytechnical University, Xi'an 710072, China

⁵School of Electronics and Information, Northwestern Polytechnical University, Xi'an 710072, China

⁶School of Biomedical Engineering, ShanghaiTech University, Shanghai 201210, China

⁷Lingang Laboratory, Shanghai, 200031, China

⁸Shanghai United Imaging Intelligence Co., Ltd.

⁹Shanghai Clinical Research and Trial Center

Abstract

Medical images and radiology reports are essential for physicians to diagnose medical conditions, emphasizing the need of quantitative analysis for clinical decision-making. However, the vast diversity and cross-source heterogeneity inherent in these data have posed significant challenges to the generalizability of current data-mining methods. Recently, multimodal large language models (MLLMs) have revolutionized numerous domains, significantly impacting the medical field. Notably, Gemini-Vision-series (Gemini) and GPT-4-series (GPT-4) models have epitomized a paradigm shift in Artificial General Intelligence (AGI) for computer vision, showcasing their potential in the biomedical domain. In this study, we evaluated the performance of the Gemini, GPT-4, and 4 popular large models for an exhaustive evaluation across 14 medical imaging datasets, including 5 medical imaging categories (dermatology, radiology, dentistry, ophthalmology, and endoscopy), and 3 radiology report datasets. The investigated tasks encompass disease classification, lesion segmentation, anatomical localization, disease diagnosis, report generation, and lesion detection. Our experimental results demonstrated that Gemini-series models excelled in report generation and lesion detection but faces challenges in disease classification and anatomical localization. Conversely, GPT-series models exhibited proficiency in lesion segmentation and anatomical localization but encountered difficulties in disease diagnosis and lesion detection. Additionally, both the Gemini series and GPT series contain models that have demonstrated commendable generation efficiency. While both models hold promise in reducing physician workload, alleviating pressure on limited healthcare resources, and fostering collaboration between clinical practitioners and artificial intelligence technologies, substantial enhancements and comprehensive validations remain imperative before clinical deployment.

*Co-first authors.

†Co-second authors.

‡Corresponding author. E-mail: xzhang@nwpu.edu.cn

1 Introduction

Recent advancements in natural language processing (NLP) have shifted from monomodal (i.e., text-only) to multimodal large language models (MLLMs), marking a significant paradigm shift in artificial general intelligence (AGI) research. To begin with text, language has always been a distinguishing feature of human intelligence from animals'. With the advancement of artificial intelligence (AI), particularly in the field of NLP, machines are becoming increasingly capable of understanding and processing language. Over the past few years, pre-trained language models (PLMs) based on self-attention mechanisms and the Transformer framework [93] have emerged and rapidly gained popularity. PLMs can learn general language representations from large-scale data in an unsupervised manner, which facilitates various downstream NLP tasks without the need for retraining new models [27]. It is noteworthy that when the scale of training data and parameters exceeds a certain threshold, language models exhibit significant performance improvements and acquire capabilities absent in smaller models, such as context learning. We refer to such models as large language models (LLMs). Large language models (LLMs) like GPT-3 [8] and its derivatives (e.g., InstructGPT [64], also known as ChatGPT), Llama series (i.e., Llama [88], Llama 2 [89], and Llama 3 [2]), and PaLM series (i.e., PaLM [16] and PaLM 2 [5]), have laid the groundwork by demonstrating exceptional text interpretation and generation capabilities [120].

The advent of the era of LLMs has brought us closer to the dawn of AGI [25, 48]. Academia and industry are experiencing vibrant competition and diverse developments, from the early Google T5 model [71] to the highly acclaimed OpenAI's GPT series today. The parameter scales of these models have long surpassed the billion-level mark, and their generative and learning capabilities of LLMs are revealing emergent abilities [100] and increasing being applied across various sectors. LLMs have demonstrated exceptional proficiency in understanding and generating natural language, providing foundational solutions for specific domains such as law [15, 19, 30], education [29, 60, 81], and public healthcare [52, 56, 115]. However, each domain deals with unique challenges, and directly using pre-trained LLMs may not yield ideal results. Fine-tuning these models, considering their inherent complexity, enables them to better adapt to downstream tasks, which is a key approach to leveraging large models [107, 119, 122].

Despite their exceptional proficiency in zero/few-shot reasoning in most NLP tasks, LLMs face challenges in processing visual information as they can only understand discrete text. Meanwhile, large-scale visual foundation models have made significant advancements in perception, leading to the gradual integration of monomodal LLMs and visual models, ultimately giving rise to the emergence of MLLMs [95]. MLLMs are models based on LLMs that can receive and reason with multimodal information, extending beyond the traditional single "language modality" to include "image," "speech," and other "multimodal" data. Among these, Gemini [4] and GPT-4 [1] are notable examples. Gemini combines language and visual information processing, while GPT-4 enhances the understanding and generation of visual data, garnering widespread attention. From the perspective of developing AGI, MLLMs may represent a step forward compared to LLMs, as they align more closely with human ways of perceiving the world, are more user-friendly, and generally support a broader range of tasks [109].

However, the exploration of these models' abilities to integrate and interpret visual data, particularly in highly specialized domains such as biomedicine, signifies a new frontier in AI application. Notable among these advancements are the GPT-4-series and Gemini-Vision-series models (namely GPT-4 and Gemini for the rest of this article), which epitomize the fusion of linguistic and visual information processing.

This research conducts a meticulous comparative analysis of GPT-4 and Gemini, focusing on their application in biomedical image analysis. And we also design experiments on the popular models including Yi, Claude, and Llama 3, to evaluate these LLMs’ textual comprehension and MLLMs’ multimodal comprehension compared to GPT-4 and Gemini. GPT-4, an advanced extension of the monomodal ChatGPT model from OpenAI, and Gemini, a similarly advanced multimodal model from Google DeepMind, are designed to comprehend and analyze information across textual and visual dimensions. This study explores how effectively these multimodal models can handle the complexities of visual data within the biomedical domain, potentially broadening their applicability and effectiveness.

The evaluation methodology includes a series of rigorous tests to assess the models’ accuracy, efficiency, and adaptability in interpreting and leveraging visual information for biomedical purposes. By examining the performance of GPT-4 and Gemini in tasks such as medical image classification, anomaly detection, and data synthesis, this paper highlights each model’s strengths and limitations. Additionally, it offers insights into optimizing these MLLMs for specialized applications.

This investigation not only showcases the groundbreaking potential of integrating advanced AI models like GPT-4 and Gemini into biomedical analysis but also sets a benchmark for future research in the field. By comparing these models, the study provides valuable knowledge to the ongoing discourse on enhancing AI’s multimodal capabilities, especially in sectors where combining text and visual data is crucial. This research underscores the transformative impact these advancements could have on medical diagnostics, treatment planning, and the broader biomedical field, marking a significant step toward realizing fully integrated AGI systems in specialized domains. Overall, the main contributions of our work are summarized as follows:

1. We provide a detailed comparative analysis of GPT-4 and Gemini models, specifically focusing on their application in biomedical image analysis, highlighting their strengths and limitations across multiple tasks such as disease classification, lesion segmentation, and report generation.
2. Our study employs rigorous evaluation methodologies to assess the accuracy, efficiency, and adaptability of these models in interpreting and leveraging visual information, offering insights into their potential optimization for specialized biomedical applications.
3. By integrating advanced AI models into biomedical analysis, our research underscores their transformative impact on medical diagnostics, treatment planning, and the broader biomedical field, setting a benchmark for future AGI system developments in specialized domains.

2 Related work

2.1 Large Language Models

With the increasing GPU computing ability and training data size, a series of Transformer [93] based pre-trained LLMs have emerged. Pre-trained LLMs can be grouped into encoder based [21, 37, 39, 49], decoder based [9, 22, 88, 117], and encoder-decoder based models [18, 39, 72, 85]. Encoder based LLMs are better at analyzing and classifying text content, including semantic feature extraction and named entity recognition. The first encoder based pre-trained LLM is the Bidirectional Encoder Representations from Transformers (BERT) [21]. BERT uses bidirectional language encoders with specially designed context-aware and mask prediction tasks on large-scale unlabeled text data. Following BERT [21], roBERT [49] further improves the performance by updating its training method, such as expanding the batch size, training on larger data, and eliminating BERT’s next-sentence

prediction task training method.

Although encoder based LLMs can effectively extract sentence features, they can not perform well on zero-shot or few-shot tasks, which are vital for LLMs. Generative Pre-trained Transformer (GPT) in the other view, uses the auto-regressive task for training and acquires better generalization ability in both zero-shot and few-shot tasks [96]. Decoder based models use the similar multi-head self-attention mechanism to the one in the encoder, but the attention mask prevents the model from attending to future positions, ensuring that the predictions for position i can only depend on the known outputs at positions less than i . Radford et al. find the scaling (model size, dataset size or both) can largely improve the decoder-based LLMs capacity [70]. This makes decoder framework widely used in scaling LLMs (ChatGPT as the most typical example). Although the scaling LLMs are based on similar deep learning architecture and training algorithm compared with smaller LLMs, they exhibit new emergent capabilities that do not appear before. For example, GPT-3 [9] can solve few-shot tasks through in-context learning, whereas GPT-2 cannot do well. Another remarkable application of scaling LLMs is ChatGPT that adapts the LLMs for dialogue, which presents an amazing conversation ability with humans and can solve different complex tasks by *instruction – tuning* [63] and *chain – of – thought* (CoT) [101]. With instruction tuning, LLMs are enabled to follow the task instructions for new tasks without using explicit examples, thus having an improved zero-shot ability which is vital for solving different tasks. CoT strategy can ease the model solving the difficult task by dividing it into multiple reasoning steps, then, LLMs can solve such tasks by utilizing the prompting mechanism that involves intermediate reasoning steps for deriving the final answer.

There are also works [18, 39, 72, 85] trying to build encoder-decoder based LLMs to take full advantage of encoder and decoder based LLMs. Encoder-decoder based LLMs are mainly used to handle tasks that require precise mapping between input and output, such as machine translation, text summarization, etc. In these tasks, it is very important to understand the precise content of the input and generate specific output accordingly. Models trained based on this architecture can generally only be applied to certain specific tasks. For example, an encoder-decoder LLM specially trained for machine translation may not be suitable for direct use in text summarization or other types of tasks. This makes encoder-decoder based LLMs mostly used in specific field, instead of the general domain like decoder based LLMs.

To summarize, with scaling model and dataset, the zero-shot and few-shot become key capabilities for LLMs. The decoder based LLMs have greater flexibility compared with encoder and encoder-decoder based LLMs. Models trained based on decoder only architecture can handle many different types of text generation tasks, such as question and answer, translation, etc., without the need for special training or adjustment for each task, thus making it more general in the practical.

2.2 Multimodal Large Language Models

In recent years, LLMs have achieved significant progress [120]. By scaling up model and data sizes, LLMs have demonstrated extraordinary emergent abilities, such as instruction following [66], in-context learning [9], and chain-of-thought reasoning [101]. Concurrently, Large Vision Models (LVMs) have also made substantial advancements [36, 62, 79, 113]. MLLMs, as a natural extension, leverage the complementary strengths of LLMs and LVMs [109].

MLLMs typically consist of a modality encoder, a pre-trained LLM, and a modality interface that bridges the gap between different modalities [109]. The modality encoder processes inputs from various modalities, such as images, videos, and audio, transforming them into representations that

the LLM can comprehend. The pre-trained LLM is responsible for understanding and reasoning over these representations. The modality interface serves as a bridge, aligning and fusing information from different modalities into the LLM.

The training process of MLLMs generally involves three stages: pre-training to align modalities and learn multimodal knowledge, instruction tuning to enable generalization to new tasks, and alignment tuning to adapt the model to specific human preferences [109]. During the pre-training stage, researchers utilize large-scale image-text paired datasets, such as LAION [77] and CC [11, 78], to train the model to learn the alignment between different modalities and acquire rich world knowledge. In the instruction tuning stage, the model is fine-tuned on instruction datasets, such as LLaVA-Instruct [43] and ALLaVA [13], to enhance its generalization ability to new tasks. During the alignment tuning stage, the model is trained using human feedback data, such as LLaVA-RLHF [83] and RLHF-V [110], to better adapt to human preferences and generate more accurate outputs with fewer hallucinations.

In addition to these open-source MLLMs, several commercial companies have introduced powerful closed-source models, such as OpenAI’s GPT-4 [61], Anthropic’s Claude-3 [6], and Microsoft’s KOSMOS-1 [67]. These models have demonstrated remarkable capabilities in handling multimodal tasks, such as generating stories based on images and performing mathematical reasoning without OCR. Their emergence has greatly promoted the development of MLLMs and provided new ideas and directions for researchers in the field.

To evaluate and compare the performance of different MLLMs, researchers have developed various benchmarks and methods. For closed-set problems (i.e., limited answer options), benchmarks such as MME [24], MMBench [47] and MM-VET [111] provide comprehensive and fine-grained quantitative comparisons. For open-set problems (i.e., flexible and diverse answer options), evaluation methods such as human scoring [125], GPT scoring [108] and case studies [102] offer qualitative analyses of MLLMs’ generative capabilities from different perspectives.

2.3 Medical MLLMs

Quality healthcare services are the cornerstone of social welfare. With increasing demand for high-quality healthcare services, the scarcity of medical resources has become a pressing issue that underscores the importance of intelligent healthcare. The creation of foundation models has garnered significant attention in the medical AI system development realm [55, 104, 116]. Compared with monomodal medical models, including medical LLMs [55] and LVMs [80], medical MLLMs that fuse various modalities have the ability to adaptively interpret and address various medical problems in different modalities, showcasing extensive applications and immense potential in the healthcare domain. By integrating language, images, audio, and other modalities of information, these models, covering medical images, electronic medical records, findings, etc. medical modalities, can offer more comprehensive and precise diagnostic, therapeutic, and patient management solutions [124]. As large models continue to evolve, notable medical MLLMs like Med-Gemini [76] have emerged.

This multimodality processing ability makes medical MLLMs more practical in clinical stages as they can give more explainable diagnosis results based on different modalities, and allow more flexible interactions for both patients and doctors. Also they can mine richer medical domain knowledge from these different acquired modalities. Technically speaking, medical MLLMs can be divided into two kinds of models, which are multimodality-alignment models and multimodality-generation models.

Multimodality-alignment Models The multimodality-alignment models are based on the pioneer work CLIP [69]. CLIP is an image-text matching model, utilizing contrastive learning methods to generate fused representations for images and texts. Based on this, there has emerged a series of works trying to align different modalities in the medical domain by this contrastive training formulation [42, 99, 116]. Moreover, a series of works further build multimodality models based on these well align medical CLIP model for explainable diagnosis [31, 58, 87, 103, 121], segmentation [3, 45, 68], structured report generation [34, 92], etc. Although these multimodality models perform well in different downstream tasks, the lack of interaction and medical knowledge makes them cannot be flexibly used in clinical stages.

Multimodality-generation Models On the other hand, the generative multimodality foundation models can provide unstructured text reports and make full use of the rich domain knowledge from their LLM component. These models are mostly based on multimodality models [40, 44] and fine-tuned specifically on medical domain. Compared with multimodality-alignment models, these models can promise more interaction, and few-shot and zero-shot learning abilities. It can not only automatically draft radiology reports that describe both abnormalities and relevant normal findings, while also taking into account the patient’s history. These models can provide further assistance to clinicians by pairing text reports with interactive visualizations, such as by highlighting the region described by each phrase.

This distinction between multimodality-alignment models and multimodality-generation models provides a foundation for understanding their practical applications across various healthcare domains. In the field of medical modalities, the mentioned multimodal MLLMs demonstrate significant potential in the following healthcare domains:

1. **Image Diagnosis and Imaging Analysis:** MLLMs integrate textual and imaging data, excelling in medical imaging diagnostics. For instance, MLLMs can expedite the identification of conditions such as cancer and pneumonia by learning from vast medical imaging datasets and corresponding diagnostic reports. These models not only automate the analysis of CT and MRI scans but also integrate imaging analyses with patient medical histories and symptom information to provide more accurate diagnostic insights.
2. **Medical Literature and Record Analysis:** MLLMs can process and comprehend extensive medical literature, research papers, and electronic health records. In medical research, these models swiftly sift through and analyze the latest research findings, aiding healthcare providers and researchers in understanding cutting-edge treatment methods and diagnostic technologies. In clinical applications, MLLMs automatically extract and analyze critical information from patient records, supporting clinical decision-making.
3. **Medical Smart Devices:** MLLMs contribute to the development of smart medical devices and robotic systems. For example, by integrating multimodal data, MLLMs enhance the precision and safety of robotic surgeries in complex procedures. These intelligent devices can analyze real-time images and data during surgery, providing precise assistance and guidance to reduce surgical risks.
4. **Drug Development Assistance:** In drug development, MLLMs predict the efficacy and side effects of new drugs by analyzing extensive biomedical data, optimizing the drug design process. These models combine data from genetics, protein structures, drug compounds, and other modalities to enhance the efficiency and success rate of new drug development.

-
5. **Remote Healthcare and Diagnostics:** MLLMs hold significant promise in remote healthcare. By integrating video, audio, and textual data, these models support remote diagnosis and treatment, offering high-quality healthcare services to remote areas with limited medical resources. MLLMs can analyze real-time communications between doctors and patients, integrating imaging and medical record data to provide accurate diagnostic recommendations.

However, most of medical MLLMs are still trained on specific disease or medial domains, making them lacking of the generality and thus cannot be a universal multimodal model for different diseases or tasks. Also, the limited training or fine-tuning dataset scale make them cannot be well validated. In addition, they face general challenges such as inefficient computing power and privacy risks. Therefore, while recognizing the development potential of MLLMs in healthcare, a cautious and measured approach is necessary.

2.4 Fine-tuning Methods in MLLMs

MLLMs integrate and process multiple forms of data, such as text and images, to perform complex tasks. Fine-tuning these models is crucial as it allows them to adapt to specific applications, enhancing their accuracy and efficiency. With the exponential growth in model parameters—from millions to billions—fine-tuning has become essential to leverage the full potential of pre-trained models for various downstream tasks.

Fine-tuning enables models to refine their understanding and improve performance in specific domains without requiring extensive retraining. This process is especially important in applications like visual question answering, image captioning, and multimodal translation, where precise alignment between different data modalities is required. Recent advancements in fine-tuning techniques have focused on making this process more efficient and scalable, ensuring that even large models can be fine-tuned with limited computational resources.

The importance of fine-tuning in MLLMs is underscored by the need to address issues such as catastrophic forgetting, where models lose their ability to retain previously learned information when adapting to new tasks. Additionally, fine-tuning helps in achieving better cross-modal alignment, where the integration of visual and textual data leads to a more coherent and accurate understanding of the inputs.

Parameter-Efficient Fine-Tuning Techniques Fine-tuning MLLMs can be challenging due to their large parameter size. Techniques such as Low-Rank Adaptation (LoRA) and Quantized LoRA (QLoRA) have been found effective. These methods adjust a subset of the model’s parameters, reducing computational requirements while maintaining performance. For instance, Lu et al. [54] scaled up models like LLaVA to 33B and 65B parameters, showing that parameter-efficient methods could achieve results comparable to full-model fine-tuning, especially when combined with high-resolution images and mixed multimodal data.

Additionally, Want et al. [97] proposed a non-intrusive techniques AdaLink, leaving the internal architecture unchanged and adapting model-external parameters. This method has been effective in both text-only and multimodal tasks, providing a competitive edge without the complexities of altering internal architectures.

Addressing Catastrophic Forgetting One significant challenge in fine-tuning MLLMs is catastrophic forgetting, where the model loses knowledge of previously learned tasks. Zhai et al. [112] proposed a technique, namely EMT (Evaluating Multimodality), to help in mitigating this by

treating MLLMs as image classifiers during fine-tuning. This approach has shown that early-stage fine-tuning on image datasets could improve performance across other datasets by enhancing the alignment of text and visual features. For example, continued fine-tuning of models like LLaVA on image datasets has shown improvements in text-image alignment, though prolonged fine-tuning could lead to hallucinations and reduced generalizability.

Moreover, Xu et al. [105] proposed an approach, called Child-Tuning, which updated only a subset of model parameters, has been initiated to improve generalization and efficiency. This method has been shown to outperform traditional fine-tuning techniques on various tasks, including those in the GLUE benchmark.

Fine-Grained Cross-Modal Alignment To achieve better cross-modal alignment, Chen et al. [12] introduced Position-enhanced Visual Instruction Tuning (PVIT), which integrated a region-level vision encoder with the language model. This technique ensured a more detailed comprehension of images by the MLLM and promoted efficient fine-grained alignment between vision and language modules. This method used multiple data generation strategies to construct a comprehensive image-region-language instruction dataset, leading to improved performance on multimodal tasks. For example, PVIT has demonstrated significant improvements in tasks requiring detailed visual comprehension, such as object detection and image segmentation.

Furthermore, techniques like LongLoRA, proposed by Chen et al. [14], have been developed to extend the context sizes of pre-trained large language models efficiently. LongLoRA combined improved LoRA with shifted sparse attention to enable context extension with significant computational savings, proving effective for tasks requiring long-context understanding.

Innovative Fine-Tuning Approaches Several innovative fine-tuning approaches have been proposed to enhance MLLMs. For example, Yang et al. [106] adopted Prompt Tuning as a lightweight and effective fine-tuning method. This approach involved fine-tuning prompts instead of the entire model, allowing for efficient adaptation to various tasks. Prompt Tuning has been shown to achieve comparable performance to full-model fine-tuning while offering improved robustness against adversarial attacks.

Another innovative approach, SCITUNE, proposed by Horawalavithana et al. [28], aligned LLMs with scientific multimodal instructions. By training models like LLaMA-SciTune with human-generated scientific instruction datasets, SCITUNE improved performance on science-focused visual and language understanding tasks.

2.5 Large Language Model Reasoning

Large language models have achieved remarkable success in a wide range of natural language processing tasks [31, 55, 58, 87, 103, 104, 116, 121], including language translation, sentiment analysis, and text classification. However, these models are typically designed to perform specific tasks, rather than engage in more general reasoning and inference. In contrast, human language understanding involves the ability to reason about complex relationships between entities, events, and concepts.

One of the key breakthroughs in large language models and reasoning is the development of cognitive architectures. These architectures are designed to mimic the human brain’s ability to process and integrate information from multiple sources, enabling models to reason and draw conclusions in a more human-like way. For example, researchers [86] at Google have developed a cognitive architecture

called "Reasoning Networks" that uses a combination of neural networks and symbolic reasoning to solve complex problems.

Recent breakthroughs [98, 118] have demonstrated the potential of large language model reasoning. 1) Engaging in multi-hop reasoning can reason about complex relationships between entities and concepts, enabling applications such as question answering and text classification. 2) Reason about cause-and-effect relationships can accurately identify in text format, enabling applications such as event extraction and text summarization. 3) Another significant advancement in large language models and reasoning is to use graph-based models, which represent language as a network of entities and relationships. These models can be trained using a variety of techniques, including reinforcement learning and adversarial training [114], which are specifically designed to test the model's robustness and ability to reason in the face of uncertainty.

In conclusion, recent advancements in large language models and reasoning have propelled the field towards more nuanced and sophisticated understanding of natural language. By leveraging cognitive architectures inspired by human cognition, researchers have made strides in enabling models to engage in multi-hop reasoning and infer cause-and-effect relationships. Additionally, the adoption of graph-based models has provided a promising avenue for representing language as interconnected entities and relationships, further enhancing the model's ability to reason across complex scenarios. Moving forward, continued research in explainability, exploration of diverse reasoning paradigms, and robustness testing will be crucial in unlocking the full potential of large language models to tackle real-world challenges and emulate human-like reasoning capabilities.

2.6 Evaluation of MLLMs

Evaluating MLLMs, is a critical aspect of understanding their capabilities and limitations. The evaluation process encompasses a range of benchmarks, metrics, and frameworks designed to assess various aspects of these models. However, the complexity and diversity of tasks that MLLMs can perform pose significant challenges to developing comprehensive and effective evaluation methodologies.

In terms of current methods for evaluating MLLMs, one of the primary benchmarks for evaluating MLLMs is the General Language Understanding Evaluation (GLUE) benchmark, which includes a suite of tasks such as sentiment analysis, textual entailment, and question answering. The SuperGLUE benchmark extends this by including more challenging tasks. For multimodal models, benchmarks such as Visual Question Answering (VQA) and the COCO dataset, which assesses image captioning, are commonly used. These benchmarks provide a standardized way to compare model performance across different tasks and modalities [10].

The evaluation of MLLMs employs various metrics to measure performance. Common metrics include accuracy, F1 score, precision, and recall for classification tasks. For generation tasks, metrics such as BLEU, ROUGE, and METEOR are used to assess the quality of text generation. In multimodal tasks, metrics like Mean Reciprocal Rank (MRR) and Intersection over Union (IoU) are used to evaluate model performance on tasks like image captioning and object detection. These metrics help quantify the performance of MLLMs on specific tasks, providing a basis for comparison [120].

Several frameworks have been developed to facilitate the evaluation of MLLMs. The Hugging Face Transformers library, for instance, includes tools for benchmarking models on a variety of tasks using pre-defined datasets. Another notable framework is EVAL, which focuses on the automatic evaluation of language models' capabilities in following natural language instructions. These frameworks streamline the evaluation process and ensure consistency in how different models

are assessed [94].

However, despite the availability of benchmarks and metrics, evaluating MLLMs presents several challenges. One major issue is the lack of standardized evaluation methods for emerging tasks. For instance, the ability of models to handle complex, multi-turn dialogues or generate contextually relevant responses in diverse scenarios is difficult to quantify with existing metrics. Additionally, the phenomenon of catastrophic forgetting, where a model loses knowledge of previously learned tasks when fine-tuned for new ones, complicates the evaluation of MLLMs’ long-term capabilities [112]. Another challenge is the evaluation of ethical considerations and biases. LLMs can inadvertently generate harmful or biased content, making it essential to assess their outputs for ethical implications. Current evaluation frameworks often fall short in systematically addressing these issues, highlighting the need for more sophisticated evaluation tools that can detect and mitigate biases and ethical risks [26].

Future research in the evaluation of MLLMs should focus on developing more comprehensive and robust benchmarks that encompass a wider range of tasks and modalities. There is also a need for better evaluation metrics that can capture the nuances of model performance in real-world applications. Additionally, incorporating human-in-the-loop evaluations can provide more accurate assessments of model performance, particularly for tasks that require nuanced understanding and interpretation. The development of evaluation platforms that integrate multiple dimensions of assessment, including performance, safety, and ethical considerations, will be crucial. These platforms should facilitate continuous evaluation as models evolve, ensuring that they remain reliable and effective in diverse applications.

3 Methodology

3.1 Datasets

3.1.1 Medical imaging tasks

In this study, we employ a diverse array of eleven distinct medical image datasets to facilitate our investigation. To provide a comprehensive comparison of multimodal large language models, we meticulously selected medical image datasets spanning five different fields. The datasets identified and incorporated in our study include iChallenge GON, MICCAI2023 Tooth Segmentation 2D, ChestXRy2017 [35], COVID-QU Ex Dataset [17, 20, 73, 84], CholecSeg8k [91], CVC ClinicDB [7], Kvasir SEG [32], m2caiSeg [57], Skin Cancer ISIC [75], Skin Cancer MNIST: HAM10000 [90], and Skin Cancer Malignant vs. Benign.

Dataset Summary:

1. **iChallenge GON** comprises a total of 1200 color fundus photographs, all stored in JPEG format. Within this dataset, 400 images are designated for glaucoma classification, while the remaining 800 images are allocated for tasks such as optic disc detection and segmentation, along with central fovea localization. In our testing task, we utilized this dataset to comprehensively investigate the capacity of large language models in glaucoma diagnosis and optic disc localization, achieved through the design of tailored prompts.
2. **MICCAI2023 Tooth Segmentation 2D** sourced from the MICCAI2023 Challenge, comprises 3000 labeled panoramic images of teeth. Its primary objective is to facilitate researchers in accurately segmenting tooth regions utilizing deep learning methodologies. In our testing scenario, we imposed heightened requirements on the large language model. Specifically, we

partitioned the oral cavity into four distinct regions and tasked the large language model with providing the count of teeth within each region and identifying the presence of dental lesions, all under zero-shot learning conditions.

3. **ChestXRay2017** jointly developed by the University of California San Diego and the Guangzhou Women and Children’s Medical Center, comprises a vast collection of validated OCT and chest X-ray images. This dataset contains thousands of validated OCT and chest X-ray images described and analyzed in "Recognition of Medical Diagnosis and Treatable Diseases through Image Based Deep Learning". The dataset is well-suited for binary classification tasks. Utilizing this dataset, our investigation centers on scrutinizing the capacity of large language models to comprehend chest radiographic imaging for pneumonia diagnosis through the development of tailored prompts.
4. **COVID-QU Ex Dataset** assembled by researchers from Qatar University, comprises 33,920 chest X-ray (CXR) images. Among these, 11,956 cases pertain to COVID-19, while 11,263 represent non-COVID-19 infections (viral or bacterial pneumonia). Additionally, the dataset includes 10,701 ground truth lung segmentation masks, making it the largest lung mask dataset to date. In our experimental evaluation, we employed this dataset to assess the efficacy of the large language model in pneumonia diagnosis based on CXR images. Moreover, we investigated the model’s capability to differentiate between typical pneumonia and novel coronavirus pneumonia.
5. **CholecSeg8k** serves as a valuable resource for semantic segmentation tasks within endoscopic modalities. Derived from the Cholec80 dataset, it comprises 8080 meticulously annotated frames from 17 videos. These images are pixel-level annotated across 13 categories commonly encountered in laparoscopic cholecystectomy surgery. In our experimental evaluation, our focus was on assessing the image recognition and comprehension capabilities of the large language model through the formulation of inquiries concerning the image content.
6. **CVC ClinicDB** serves as the official dataset for the training phase of the MICCAI 2015 Colonoscopy Video Automatic Polyp Detection Challenge. This database comprises 612 static images extracted from colonoscopy videos, sourced from 29 distinct sequences. In our evaluation, we utilized endoscopic images of intestinal polyps from this dataset to assess the discriminative capability of the large language model for detecting intestinal polyps.
7. **Kvasir SEG** comprises 1000 polyp images along with their corresponding ground truth annotations, derived from the Kvasir Dataset v2. The resolution of images in the Kvasir-SEG dataset ranges from 332x487 to 1920x1072 pixels. The images and their corresponding masks are stored in two separate directories, each utilizing the same filenames for easy pairing. The image files are encoded using JPEG compression. In our testing, we evaluated the model’s capability in lesion detection by inputting images with lesions into the large language model.
8. **m2caiSeg** is a dataset for segmenting endoscopic images during surgery. Originating from the first and second videos of the MICCAI 2016 Surgical Tool Detection dataset, it encompasses a total of 307 images, each meticulously annotated at the pixel level. The dataset features images of diverse organs (e.g., liver, gallbladder, upper wall, intestines), surgical instruments (e.g., clips, bipolar forceps, hooks, scissors, trimmers), and bodily fluids (e.g., bile, blood). Additionally, it includes specialized labels for unknown and black regions to address areas obscured by certain instruments.
9. **Skin Cancer ISIC** comprises 2357 images of both malignant and benign oncological conditions,

curated by The International Skin Imaging Collaboration (ISIC). The images are categorized based on ISIC’s classification, with all subsets containing an equal number of images, except for those of melanomas and moles, which are slightly more prevalent. In our evaluation, we assessed the classification and recognition capabilities of the large language model for various skin diseases. Additionally, we tested the model’s ability to comprehend image content based on these classifications.

10. **Skin Cancer MNIST: HAM10000** comprises 10,015 dermoscopic images collected from diverse populations through various acquisition methods. It includes representative cases from all major diagnostic categories of pigmented lesions: actinic keratoses and intraepithelial carcinoma/Bowen’s disease (akiec), basal cell carcinoma (bcc), benign keratosis-like lesions (bkl), dermatofibroma (df), melanoma (mel), melanocytic nevi (nv), and vascular lesions (vasc). In our evaluation, we assessed the large language model’s capabilities in multi-class classification and lesion localization for various skin diseases.
11. **Skin Cancer Malignant vs. Benign** contains 1800 images of skin cancer, both malignant and benign, organized into two separate folders. Each image has a resolution of 224x244 pixels. In our experiment, we assessed the large language model’s capability to distinguish between benign and malignant skin cancer by designing specific prompts and utilizing images from the dataset.

3.1.2 Medical report generation task

In this investigation, we utilized three distinct datasets of radiology chest X-ray reports: MIMIC-CXR (publicly available) [33], OpenI (publicly accessible) [53], and SXY (privately obtained) [123]. Our analysis focused on the inspection findings and conclusion segments across these datasets. By formulating tailored prompts, we assessed the efficacy of a large language model in generating radiological text reports, with a particular emphasis on crafting conclusions derived from the examination findings.

Dataset Summary:

1. **MIMIC-CXR** represents a substantial publicly accessible repository comprising chest radiographs in DICOM format along with accompanying free-text radiology reports. This extensive dataset encompasses 377,110 images corresponding to 227,835 radiographic studies conducted at the esteemed Beth Israel Deaconess Medical Center located in Boston, Massachusetts.
2. **OpenI** provided by the National Center for Biotechnology Information (NCBI) at the National Institutes of Health (NIH), constitutes a publicly available repository of medical images sourced from scholarly literature. Predominantly comprising X-rays, CT scans, and MRI images, the dataset is accompanied by relevant metadata. Designed to facilitate advancements in medical image analysis and information retrieval, OpenI serves as a resource for researchers to train and evaluate various algorithms and techniques in the field.
3. **SXY** courtesy of Xiangya Second Hospital, affiliated with Central South University, encompasses radiology reports spanning from 2012 to 2023 across five systems. This comprehensive dataset includes essential information, detailed descriptions, and diagnostic impressions. These data serve as the foundation for model development and internal validation processes. Specifically, we leverage the chest X-ray reports for testing purposes within our study framework.

3.2 Model Selection

In this research, we mainly target on evaluating the multimodal performance of Gemini and GPT families in the biomedical region. To provide a comprehensive comparison within these families, we either consider the generation or the usage-specific type. For the Gemini family, we select Gemini-1.0-Pro-Vision, Gemini-1.5-Pro, and Gemini-1.5-Flash; for the GPT family, we adopt GPT-3.5-Turbo, GPT-4-Turbo, and GPT-4o into the model pool. Despite the extensiveness of exploring the two specified families, we have strong determination on identifying their effectiveness compared to other latest, cutting-edge, prestigious, and state-of-the-art LLMs to reflect the most practical assessment of current LLMs, not limited to only the Gemini and GPT families. Correspondingly, we supplement Yi-Large, Yi-Large-Turbo, Claude-3-Opus and Llama 3 to construct the final model pool.

Descriptions of these models are listed as follows:

1) Gemini-Pro: Google’s Gemini-Pro model is a state-of-the-art multimodal AI platform designed to excel across a wide range of tasks with high accuracy. Launched in February 2024, Gemini-Pro handles complex queries in various domains, including STEM and humanities. It features enhanced capabilities in Python code generation, challenging math problems, and multi-step reasoning tasks. Additionally, it demonstrates impressive performance in language translation and automatic speech recognition. By May 2024, its performance had further improved, reflecting Google’s commitment to advancing AI technology. In the following experiment session, we include Gemini-1.0-Pro-Vision and Gemini-1.5-Pro in the model pool.

2) Gemini-Flash: Gemini-Flash, introduced as a more streamlined version of the Gemini AI platform, is optimized for speed and efficiency. While it may not match the accuracy of Gemini-Pro, it delivers results more rapidly, making it an excellent choice for applications that require swift responses. Currently available as a public preview for developers through Google’s AI Studio, Gemini-Flash is designed to support the development of fast-paced applications and chatbots. It shares the same one million token limit as Gemini-Pro, ensuring that it can process substantial amounts of data, albeit with a slightly lower accuracy in benchmark tests. In the following experiment session, we include Gemini-1.5-Flash in the model pool.

3) GPT-4o: OpenAI’s latest flagship model, GPT-4o, marks a significant advancement in human-computer interaction by processing and generating text, audio, and visual content in real time. This "omni" model excels in handling diverse inputs and outputs, including speech and images, with response times averaging 320 milliseconds, closely mirroring human conversational pace. Additionally, GPT-4o’s multilingual capabilities have been greatly enhanced, offering improved performance in understanding non-English text, vision, and audio. Despite these advancements, GPT-4o remains more cost-effective and faster in API usage compared to its predecessors.

4) GPT-4-Turbo: The predecessor to GPT-4o, GPT-4-Turbo, is an enhanced version of the GPT-4 model line. It features a 128k context window, enabling it to process substantial amounts of text—up to 300 pages in a single prompt. Updated with knowledge up to April 2023, GPT-4-Turbo is more affordable, offering reduced costs for both input and output tokens, with a maximum output token limit of 4096. This model is accessible to any OpenAI API account holder with existing GPT-4 access and can be specified by using gpt-4-turbo as the model name in the API.

5) GPT-3.5-Turbo: GPT-3.5-Turbo is a powerful iteration in OpenAI’s language model series, designed to offer a balance between performance and efficiency. It provides robust text generation and comprehension capabilities with a focus on cost-effectiveness and speed. The model can handle a wide range of language tasks, including summarization, translation, and question-answering, making it versatile for various applications. Despite being less advanced than the GPT-4 series, GPT-3.5-Turbo remains a reliable and accessible option for many users, maintaining strong performance while being more affordable for large-scale deployments.

6) Yi: Yi is an advanced open-source large language model developed by 01.AI. Available in two versions, Yi-34B and Yi-6B, it supports bilingual capabilities (English and Chinese) and is designed for both academic research and commercial use with appropriate licensing. Yi-34B, with its 34 billion parameters, excels in numerous benchmarks such as MMLU, CMMLU, and C-Eval, outperforming many larger models like Llama-2 70B. It offers an impressive context window of 200K, enabling it to handle extensive text inputs effectively. In the following experiment session, we contain Yi-Large and Yi-Large-Turbo in the model pool.

7) Claude-3-Opus: Claude-3-Opus, developed by Anthropic, excels in handling complex tasks and content creation. It supports both text and image inputs, making it versatile for multimodal applications. With a context window of 200K, it can manage extensive inputs efficiently, and its output quality is tailored for high-level fluency and understanding. This model balances speed and intelligence, making it suitable for tasks requiring nuanced comprehension and detailed responses. We select Claude-3-Opus, part of Anthropic’s Claude family, which includes several models designed to cater to varying needs of performance and cost-effectiveness, in the final model pool.

8) Llama 3: Llama 3, developed by Meta, represents a significant advancement in open-source large language models. It includes models with 8 billion and 70 billion parameters, designed for a wide range of applications. Llama 3 improves upon its predecessors with enhanced pre-training data, a more efficient tokenizer, and advanced instruction fine-tuning techniques. It supports extensive context windows and demonstrates state-of-the-art performance in benchmarks such as reasoning, coding, and content creation. Meta aims to foster innovation by making Llama 3 widely available and emphasizing responsible use and deployment.

3.3 Experiment Setting

To more rigorously evaluate the proficiency of various large language models (LLMs) in handling medical images and reports under zero-shot conditions, we segmented the testing experiment into two distinct phases: testing of medical image data and testing of medical report generation, as illustrated in **Fig. 1(a)**.

In order to ascertain the fairness and reliability of the experiment, we carried out experimental trials across diverse models using identical parameter configurations. Our testing methodology involves employing a standardized set of prompts and parameters to evaluate the performance of the LLM.

When conducting medical image testing, we rigorously observe the prescribed usage protocols for each model. As shown in **Fig. 1(b)**, We perform medical image testing utilizing models like GPT-4-Turbo and Claude-3-Opus through the web interface. However, owing to the stringent content restrictions of Gemini-series models on the web platform, it is unable to participate in equitable competition with other models in the medical imaging domain. Consequently, we opted to utilize the Google AI Studio platform for conducting medical image testing on Gemini-series models. In

order to comprehensively assess the interpretive capabilities of various models within the medical imaging domain, we meticulously crafted distinct prompts tailored to specific datasets and tasks. Uniform prompts and input images were employed across all tests for different models to ensure the integrity and fairness of the results.

During the testing of medical report generation, given the extensive volume of tests, Python was employed to invoke the open API interfaces of various models on the Colab platform. Throughout the testing phase, consistency between the prompts utilized and the model inputs was maintained to produce a series of results, subsequently evaluated for efficacy.

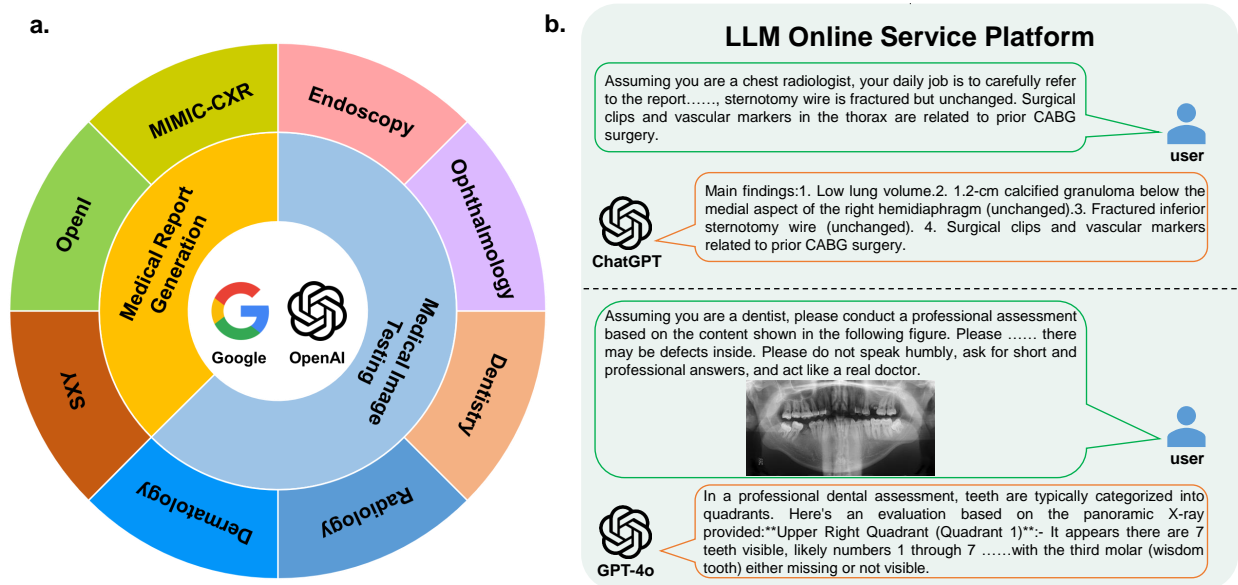


Figure 1: **Schematic Overview of the Evaluation Tasks and Methods.** (a). The core of the graph delineates the two focal tasks of our evaluation model, while the specific datasets or evaluation subjects pertinent to each task are outlined along its periphery. (b). Our testing tasks were executed by formulating suitable prompts and leveraging the online Language Model service offered by OpenAI and Google.

3.4 Evaluating Indicator

In the task of medical image question answering, our research rigorously juxtaposed responses from various large-scale models when presented with identical input images and queries. For diverse medical images, we employed ground truth supplied in the dataset, such as semantic segmentation maps and optic disc segmentation maps, as benchmark answers. This enabled a comprehensive horizontal comparison of responses generated by different language models, facilitating the synthesis of the respective strengths and weaknesses of each model.

In the context of generating radiology reports, our approach involves employing the ROUGE [41] (Recall-Oriented Understudy for Gisting Evaluation) metric to assess the level of correspondence between radiology reports generated by the large language model and the reference answers authored by medical professionals. This study incorporates three distinct methods: Rouge-1 (R-1), Rouge-2 (R-2), and Rouge-L (R-L), as shown from Eq. (1).

$$ROUGE - N = \frac{\sum_{S \in \{ReferenceSummaries\}} \sum_{gram_n \in S} Count_{match}(gram_n)}{\sum_{S \in \{ReferenceSummaries\}} \sum_{gram_n \in S} Count(gram_n)} \quad (1)$$

4 Experiments and Observation

4.1 Medical Image Test Results

In **Section 4.1.1**, we evaluated the performance of six advanced multimodal large language models, including GPT-4-Turbo, across five distinct categories of medical imaging question answering. For the chest X-ray dataset, our primary focus was on the models’ ability to diagnose pneumonia or other diseases from chest X-ray images. As depicted in **Fig. 2**, the GPT-series models excelled in this task, accurately determining patient health status without requiring additional prompt information. The Gemini-series models followed in performance, while Claude-3-Opus performed the worst, with its answers offering negligible reference value. It is important to note that none of the six models we assessed could further determine whether the pneumonia was COVID-19, which does not imply a lack of model performance, as distinguishing the type of pneumonia based solely on X-ray images is inherently impossible.

In **Section 4.1.2**, leveraging the ophthalmic imaging dataset, our analysis centers on the model’s ability to diagnose glaucoma and accurately identify the macular fovea’s position using fundus photographs. As depicted in **Fig. 3**, in Case 1, all models except Claude-3-Opus and GPT-4o incorrectly diagnosed the absence of glaucoma. However, regarding macular fovea localization, GPT-4-Turbo was the only model to offer a vague location, while all other models failed to provide accurate localization. In Case 2, only GPT-4o successfully detected glaucoma, and GPT-4-Turbo again provided a vague description of the macular fovea position, whereas the other models did not accomplish the task.

In **Section 4.1.3**, utilizing the endoscopic imaging dataset, our focus is on the model’s capability to describe lesion conditions in detail within complex scenes and accurately determine the lesion’s location. As illustrated in **Fig. 4**, all models successfully provided detailed descriptions of the lesions, with the GPT-series models offering the most comprehensive information. Notably, only Gemini-1.0-Pro-Vision and Claude-3-Opus were unable to determine the lesion locations, whereas the remaining models accurately identified the lesion locations.

In **Section 4.1.4**, we investigate the model’s capability to classify skin diseases using a skin disease dataset, without the aid of supplementary prompts. As demonstrated in **Fig. 5**, none of the models accurately identified the type of skin disease afflicting the patients. This deficiency may stem from the sensitivity of the skin disease images or the insufficient training of the large language model on this particular category of diseases.

In **Section 4.1.5**, employing the dental X-ray dataset, our focus is on the model’s ability to assess dental health and count the number of existing teeth. As shown in **Fig. 6**, due to the lack of accurate reference answers, our evaluation was based solely on the models’ responses. The responses from the Gemini-series models were relatively simple, concentrating only on the number of teeth. In contrast, the responses from Claude-3-Opus and the GPT-series models were more detailed, addressing tooth integrity, surrounding bone structures, the presence of implants, and the presence of wisdom teeth, while also providing relevant recommendations.

4.1.1 Chest Radiography

Prompt	Image
Assuming you are a radiologist, please conduct a professional evaluation based on the content shown in the following figure. Please describe what you see in the following picture? Judge whether the patient has pneumonia according to the figure below, and point out whether it is COVID-19. Please do not speak humbly, request short and professional answers, and behave like a real doctor.	
Reference answer	COVID-19
Gemini-1.0-Pro-Vision	
The X-ray image shows bilateral interstitial pneumonia. There is no obvious consolidation. It is not COVID-19. It is more likely to be mycoplasma pneumoniae.	
Gemini-1.5-Pro	
This is a frontal chest radiograph. There is no evidence of pneumonia or findings specific for COVID-19.	
Gemini-1.5-Flash	
This is a chest x-ray. The image shows clear lung fields bilaterally. There are no signs of pneumonia or COVID-19.	
GPT-4-Turbo	
Based on the chest X-ray provided, here is a professional radiological assessment: Observations :1. Lung Fields : There are areas of increased opacity in both lung fields, notably in the periphery. Such opacities can be indicative of an infectious process.2. Heart Size and Mediastinum : The cardiac silhouette appears normal in size. There is no evidence of widening of the mediastinum.3. Diaphragm and Pleural Spaces : The diaphragm is well visualized with no evident pleural effusion. The costophrenic angles are sharp.4. Bony Structures and Soft Tissues : No abnormalities are visible in the bony thorax or the soft tissues around the lungs. Assessment :- The pattern of peripheral opacities observed on the X-ray can be seen in cases of viral pneumonia, including COVID-19. However, the appearance on chest X-ray alone is not specific and can overlap with other types of viral pneumonias or inflammatory processes. Diagnosis :- Given the findings suggestive of an infectious process and the presentation compatible with viral pneumonia, COVID-19 is a consideration, especially in the appropriate epidemiological context. However, confirmation of COVID-19 requires specific testing, such as RT-PCR, for SARS-CoV-2. Recommendations :- - Clinical correlation with symptoms (e.g., fever, cough, difficulty breathing) and epidemiological information (exposure history, prevalence in the community) is essential.- It is recommended to perform a PCR test for COVID-19 to confirm the diagnosis. - Depending on clinical severity, further imaging such as a CT scan of the chest could be considered for more detailed evaluation.This assessment is based on the X-ray image provided and should be correlated with clinical findings for a definitive diagnosis.	
Claude-3-Opus	
Based on the chest X-ray provided, there are bilateral patchy airspace opacities present in both lungs, more prominent in the lower lung zones. The heart size appears normal. No pleural effusions are seen. Given the bilateral nature and distribution of the lung opacities, the findings are consistent with multifocal pneumonia. In the current context of the COVID-19 pandemic, these radiographic features raise the possibility of COVID-19 pneumonia, although the findings are not specific and can be seen with other viral or atypical pneumonias as well. Correlation with the patient's clinical presentation, exposure history, and laboratory testing, including COVID-19 PCR, would be necessary to make a definitive diagnosis. Close follow-up and treatment per current protocols are advised.	
GPT-4o	
Based on the chest X-ray provided:- Findings :- The image shows bilateral lung fields with some increased opacity in the lower zones, particularly on the right side.- The heart size appears within normal limits.- There are no obvious pleural effusions.- Assessment :- The increased opacity in the lower lung zones suggests a possible infection or inflammation.- This radiographic appearance can be consistent with pneumonia.- COVID-19 Evaluation :- The radiographic findings alone cannot definitively diagnose COVID-19. However, the pattern of bilateral lower lung opacities can be seen in COVID-19 pneumonia.- Further clinical correlation and testing (e.g., RT-PCR for SARS-CoV-2) are necessary to confirm COVID-19. The patient may have pneumonia, but further tests are needed to determine if it is caused by COVID-19.	

Figure 2: **Chest: Case 1.** In the context of the three-class classification tasks for pneumonia (normal, pneumonia, COVID-19), the green annotation indicates the correctly identified segments, while the red annotation denotes the incorrectly identified segments.

4.1.2 Ophthalmological Imaging

Prompt	Image
Assuming you are an ophthalmologist, please conduct a professional evaluation based on the content shown in the following figure. Please determine whether the patient has glaucoma based on fundus figure? Please estimate the coordinate position of the macular fovea, starting from the top left corner of the image as the (0,0) coordinate, increasing to the right along the x-axis and decreasing along the y-axis. Please do not speak humbly, ask for short and professional answers, and act like a real doctor.	
Reference answer	Glaucoma Fovea: (1133.61, 1084.37)
Gemini-1.0-Pro-Vision	
Based on the fundus image, the patient does not have glaucoma . The optic nerve head is normal in size and shape, and there is no evidence of optic nerve cupping or enlargement of the optic disc. The retinal nerve fiber layer is also normal in thickness. The macular fovea is located at (150, 150) .	
Gemini-1.5-Pro	
No glaucoma . Macular fovea is approximately (400,-200) .	
Gemini-1.5-Flash	
The patient does not have glaucoma . The optic nerve head appears normal with no cupping or rim thinning. The macular fovea is located at approximately (400, -200) .	
GPT-4-Turbo	
Based on the fundus photograph provided: Findings: - The image shows the posterior segment of the eye with a clear view of the optic disc, blood vessels, and surrounding retina.- Optic Disc: There is no obvious cupping or pallor of the optic disc. The optic disc appears to have a healthy pink hue with a normal cup-to-disc ratio.- Blood Vessels: The retinal blood vessels are of normal caliber and show no signs of bending or nicking.- Macula: The macular region is not highlighted with a visible fovea reflex, but the overall retinal architecture appears intact.*Glaucoma Assessment:*From the visible indicators in this image, there are no overt signs of glaucoma . Glaucoma typically manifests with increased optic disc cupping, which is not apparent here.- A definitive diagnosis for glaucoma would require additional tests such as intraocular pressure measurement, visual field testing, and an OCT scan to measure the nerve fiber layer thickness around the optic disc. Estimation of Macular Fovea Coordinates: - The macular fovea is typically located horizontally in line with the optic disc and slightly below it. Assuming the top left corner of the image as (0,0) and judging by the size and scale of the image, the macular fovea could be approximately located at:- X-coordinate: Halfway across the width of the image from the left.- Y-coordinate: Slightly lower than the centerline of the image, approximately one-third from the top of the image. Recommendations: - To rule out glaucoma or other conditions, a comprehensive eye examination including intraocular pressure measurement and visual field testing is recommended.- Follow-up with an OCT scan can provide detailed information about the optic nerve and macular health. Conclusion: The fundus image does not show typical signs of glaucoma. The estimated location of the macular fovea, based on the description, should be verified with precise measurements in a clinical setting. Further ophthalmic tests are advised to confirm the health of the optic nerve and retina.	
Claude-3-Opus	
Based on the fundus photograph provided, I can make the following assessment as an ophthalmologist:The optic disc shows focal notching and thinning of the neuroretinal rim at the inferior pole (marked by the blue circle), which is suspicious for glaucomatous optic neuropathy. The cup-to-disc ratio appears to be approximately 0.7-0.8 vertically. There are also visible retinal nerve fiber layer defects extending from the optic disc inferiorly.Given these findings, this patient likely has glaucoma in this eye. However, I would need to correlate this with additional testing like optical coherence tomography (OCT) of the optic nerve and retinal nerve fiber layer, as well as visual field testing, to confirm the diagnosis and staging.The fovea is located at approximately the coordinate (325, 240) , estimating from the top left corner of this 650x650 pixel image.In summary, this fundus photograph is highly suspicious for glaucoma , pending confirmatory testing. Close monitoring and likely treatment initiation would be warranted for this patient.	
GPT-4o	
### Evaluation of Fundus Image**Glaucoma Assessment:**Based on the fundus image provided, the optic disc appears to have a large cup-to-disc ratio. This is a common indicator of glaucoma , as the optic nerve head seems to be showing signs of cupping and thinning of the neuroretinal rim. This assessment should be confirmed with additional tests such as intraocular pressure measurement, visual field analysis, and optical coherence tomography (OCT).**Macular Fovea Position:**The macular fovea, indicated by the purple cross, is approximately located at coordinates (900, 850) in the image, assuming the top left corner is (0,0).Further clinical examination and diagnostic tests are recommended to confirm the diagnosis of glaucoma.	

Figure 3: **Ophthalmological Imaging: Case 1.** Diagnosis of glaucoma and the task of localizing the macular fovea, the green annotation indicates the correctly identified segments, while the red annotation denotes the incorrectly identified segments.

4.1.3 Endoscopic Imaging

Prompt	Image	Reference answer
<p>Assuming you are a gastroenterologist, please evaluate the lesion area and type from the image below, and provide corresponding suggestions. Please do not speak humbly, but act like a real doctor.</p>		
<p>Gemini-1.0-Pro-Vision</p>		
<p>The lesion is a large, ulcerated mass with a cauliflower-like appearance. It is located in the stomach. The most likely diagnosis is gastric cancer. The next step is to determine the stage of the cancer. This will involve additional tests, such as a biopsy and an endoscopy. The stage of the cancer will determine the best course of treatment. Treatment options for gastric cancer include surgery, chemotherapy, radiation therapy, and targeted therapy. The goal of treatment is to remove the cancer and prevent it from coming back. The prognosis for gastric cancer depends on the stage of the cancer and the patient's overall health. The earlier the cancer is diagnosed and treated, the better the prognosis.</p>		
<p>Gemini-1.5-Pro</p>		
<p>This is an image from an upper endoscopy. There is a large, ulcerated, and friable mass in the stomach. This requires biopsy, but given the appearance, malignancy is a significant concern. Depending on biopsy results, surgical resection may be indicated.</p>		
<p>Gemini-1.5-Flash</p>		
<p>This is an endoscopic image of the colon. There is a large, sessile polyp with an ulcerated surface, suggestive of a malignant lesion. This needs to be biopsied immediately. The patient will need to be scheduled for a colonoscopy with possible polypectomy to remove the polyp and have it sent for pathological examination.</p>		
<p>GPT-4-Turbo</p>		
<p>The image you provided appears to be an endoscopic view of a gastrointestinal lesion, specifically in the colon. The lesion looks like a large, ulcerated mass with irregular, nodular surfaces and areas of active bleeding. Such characteristics are concerning for a malignant tumor, possibly colorectal cancer. As a gastroenterologist reviewing this image, I would recommend the following steps: 1. Biopsy: Immediate biopsy of the lesion during the endoscopy session, if not already done, to confirm the diagnosis through histopathological examination. 2. Full Colonoscopy: If this has not been a complete colonoscopic examination, it's crucial to evaluate the entire colon for any additional lesions. 3. Imaging Studies: Conduct imaging studies such as CT or MRI scans of the abdomen and pelvis to assess for local invasion or distant metastases. 4. Referral to Oncology: Early referral to an oncologist for management planning, which might include surgery, chemotherapy, or radiation, depending on the stage and nature of the tumor. 5. Follow-up and Support: Provide the patient with information on treatment options and supportive care, including nutritional support and counseling. Immediate and thorough medical intervention is vital given the potentially serious nature of this lesion.</p>		
<p>Claude-3-Opus</p>		
<p>The image shows an endoscopic view of the stomach revealing multiple gastric polyps along the rugal folds. The largest polyp measures approximately 2-3 cm in diameter and has a lobulated, irregular surface with evidence of focal erosion or ulceration. Based on the appearance, these polyps are most consistent with hyperplastic or fundic gland polyps, which are generally benign. However, the size and irregular, eroded surface of the largest polyp is concerning for potential dysplasia or even an early gastric adenocarcinoma arising within the polyp. Given these findings, I recommend the following: 1. Biopsy multiple polyps, especially the large, irregular one, to determine the histologic type and rule out dysplasia or malignancy. 2. If biopsy confirms these are hyperplastic or fundic gland polyps, recommend surveillance endoscopy in 1-3 years to monitor for growth or changes suspicious for neoplasia. 3. If dysplasia or cancer is found, the patient will need referral to a surgeon for consideration of partial gastrectomy and staging. 4. Test and treat for H. pylori, if present, as this can contribute to polyp growth. 5. Consider screening upper endoscopy for first degree relatives over age 40, as some gastric polyp syndromes can be hereditary. Close follow-up will be important for this patient given the size and appearance of the dominant gastric polyp. Definitive diagnosis and management will depend on the pathology results from biopsies taken during this procedure.</p>		
<p>GPT-4o</p>		
<p>Based on the endoscopic image provided:- Findings: The image shows a large, irregular, ulcerated mass with areas of necrosis and bleeding. The lesion appears to be protruding into the lumen of the gastrointestinal tract.- Assessment: The appearance is highly suggestive of a malignant tumor, likely colorectal cancer given the location and characteristics.- The ulceration and irregular borders are indicative of an advanced stage lesion.- Recommendations: Biopsy: Immediate biopsy of the lesion is recommended to confirm the diagnosis and determine the histopathological type.- Staging: Further imaging (CT, MRI) and possibly PET scans to stage the cancer and assess for metastasis.- Multidisciplinary Evaluation: Consultation with oncology, surgery, and potentially radiation therapy to discuss treatment options which may include surgery, chemotherapy, and/or radiation therapy.- Follow-Up: Regular follow-up and monitoring for response to treatment and potential complications. Prompt action is necessary to confirm the diagnosis and initiate appropriate treatment.</p>		

Figure 4: **Endoscopic: Case 1.** The task of colon polyp localization and segmentation uses green markings to represent correct answers, red markings to represent incorrect answers, and yellow markings to highlight noteworthy content.

4.1.4 Dermatological Imaging

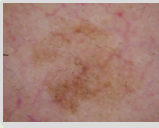
Prompt	Image
Assuming you are a dermatologist, please conduct a professional evaluation based on the content shown in the following figure. Is there any lesion in the following picture? If so, please provide a brief description of the lesion and explain what it is. Please do not speak humbly, ask for a brief and professional answer, and act like a real doctor.	
Reference answer	actinic keratosis
Gemini-1.0-Pro-Vision	
There is a pigmented lesion on the patient's back. It is round, with a diameter of about 6 mm. The color is light brown, and the borders are irregular. The surface is smooth, and there is no scaling or crusting. This lesion is most likely a seborrheic keratosis . Seborrheic keratoses are common, benign growths that are found in older adults. They are caused by an overgrowth of the cells in the epidermis, the outer layer of the skin. Seborrheic keratoses are typically harmless, and they do not require treatment. However, they can sometimes be mistaken for skin cancer, so it is important to have them checked by a dermatologist if you are concerned.	
Gemini-1.5-Pro	
Yes, there is a lesion in the picture. This is a pigmented lesion with irregular borders and color variation, suspicious for melanoma . It needs to be biopsied.	
Gemini-1.5-Flash	
There is a lesion in the image, it appears to be a seborrheic keratosis , a common, noncancerous skin growth. It is characterized by its brown, waxy, and slightly raised appearance.	
GPT-4-Turbo	
The image provided appears to be a dermoscopy photo, a technique used in dermatology to examine skin lesions with a dermatoscope. Here's a professional evaluation based on the image: Observation : The lesion depicted in the image shows a complex pattern with multiple colors including shades of brown and black, and a pinkish hue in the background. There are irregular pigment networks and possible structural changes within the lesion. Assessment : The presence of multiple colors and irregular structures suggests this could be a melanocytic lesion . The asymmetry and color variation may raise a concern for melanoma, a type of skin cancer that arises from melanocytes. Diagnosis : This lesion has characteristics that could be indicative of melanoma, including asymmetry, border irregularity, color variation, and a diameter that seems larger than 6 mm (based on the scale shown). Recommendations : A clinical evaluation is necessary to assess the lesion further. I recommend an excisional biopsy to ensure accurate diagnosis. Histopathological examination of the biopsy will confirm whether this is benign, like a dysplastic nevus, or malignant, such as melanoma. Conclusion : Due to the suspicious nature of the lesion seen in the dermoscopy image, prompt dermatological consultation and possible biopsy are advised to rule out melanoma and to guide appropriate management.	
Claude-3-Opus	
Based on the image provided, there appears to be a lesion present on the skin. The lesion has the following characteristics:- Irregular, asymmetrical shape- Mottled, patchy coloration ranging from light to dark brown- Slightly raised and rough texture compared to surrounding skin Given these visual characteristics, this lesion is most consistent with a pigmented nevus , commonly known as a mole. Moles are benign growths formed by clusters of melanocytes, the pigment-producing cells in the skin. While the majority of moles are harmless, it's important to monitor any changes in size, shape, color, or texture. Sudden or progressive changes could be potential signs of malignant transformation, such as melanoma. I recommend performing regular self-examinations and having any concerning moles evaluated by a dermatologist for a more definitive diagnosis and appropriate management.	
GPT-4o	
Based on the dermoscopic image provided:- Findings : There is an irregular, pigmented lesion with varying shades of brown.- The lesion exhibits an asymmetric pattern with irregular borders.- There are areas of pigmentation that vary in color and density.- Assessment : The appearance is concerning for a potential melanoma , given the asymmetry, irregular borders, and heterogeneous pigmentation.- Further evaluation, including a biopsy, is recommended to confirm the diagnosis and rule out malignancy. The lesion shows features suggestive of melanoma, warranting prompt further investigation.	

Figure 5: **Skin: Case 1.** The nine classification tasks for skin diseases utilize green markings to denote correct answers and red markings to indicate incorrect answers.

4.1.5 Dental Imaging

Prompt	Image
Assuming you are a dentist, please conduct a professional assessment based on the content shown in the following figure. Please divide the teeth in the following image into four regions: upper right region, upper left region, lower left region, and lower right region. Please accurately state the number of teeth in each area of the picture, as there may be defects inside. Please do not speak humbly, ask for short and professional answers, and act like a real doctor.	
Reference answer	No reference information
Gemini-1.0-Pro-Vision	
Upper right region: 7 teeth. **Upper left region:** 6 teeth. **Lower left region:** 5 teeth. **Lower right region:** 6 teeth. **Total:** 24 teeth. There are 24 teeth in total , with 7 in the upper right region, 6 in the upper left region, 5 in the lower left region, and 6 in the lower right region. There are no obvious signs of pathology.	
Gemini-1.5-Pro	
Upper right: 8 teeth Upper left: 8 teeth Lower left: 8 teeth Lower right: 8 teeth	
Gemini-1.5-Flash	
Upper right region: 5 teeth Upper left region: 5 teeth Lower left region: 6 teeth Lower right region: 5 teeth	
GPT-4-Turbo	
Based on the panoramic dental X-ray provided, here is a professional assessment of the dental structures visible: **Upper Right Region (Quadrant 1)** **Number of Teeth:** 8 teeth are visible, including the wisdom tooth (third molar). All teeth appear present from the second molar to the central incisor. **Upper Left Region (Quadrant 2)** **Number of Teeth:** 8 teeth are visible, including the wisdom tooth. This quadrant also appears to have all teeth present from the central incisor to the third molar. **Lower Left Region (Quadrant 3)** **Number of Teeth:** 7 teeth are visible. It appears that the third molar (wisdom tooth) is missing, with all other teeth from the second molar to the central incisor present. **Lower Right Region (Quadrant 4)** **Number of Teeth:** 7 teeth are visible. Similar to the lower left, the third molar is absent, and all other teeth from the central incisor to the second molar are visible. **Overall Assessment:** - All quadrants display typical dental alignment without obvious signs of crowding or significant dental pathologies on this X-ray. However, the absence of third molars in the lower quadrants is noted. No overt signs of major decay or large restorations are visible in this radiograph, although clinical examination and additional focused X-rays are recommended for a thorough evaluation, particularly for caries detection under the gumline or between teeth. This assessment provides a basic overview based on the X-ray provided; however, a complete dental evaluation would require a clinical examination and possibly more focused radiographs.	
Claude-3-Opus	
Based on the dental X-ray provided, here is my professional assessment of the teeth in each region: Upper right region (UR): 8 teeth visible - central incisor, lateral incisor, canine, 1st and 2nd premolars, 1st, 2nd and 3rd molars. No obvious defects or pathologies noted. Upper left region (UL): 8 teeth visible - central incisor, lateral incisor, canine, 1st and 2nd premolars, 1st, 2nd and 3rd molars. No obvious defects or pathologies noted. Lower left region (LL): 8 teeth visible - central incisor, lateral incisor, canine, 1st and 2nd premolars, 1st, 2nd and 3rd molars. No obvious defects or pathologies noted. Lower right region (LR): 8 teeth visible - central incisor, lateral incisor, canine, 1st and 2nd premolars, 1st, 2nd and 3rd molars. No obvious defects or pathologies noted. In summary, the patient has a full complement of 32 teeth with no discernible defects or pathologies based on this panoramic radiograph. Further clinical examination and additional imaging may be necessary to confirm the absence of any dental issues.	
GPT-4o	
### Dental Panoramic X-ray Assessment **Upper Right Region:** - Number of teeth: 6- Observation: Includes molars, premolars, and anterior teeth. The presence of third molars (wisdom teeth) should be noted. **Upper Left Region:** - Number of teeth: 6- Observation: Similar to the upper right, including molars, premolars, and anterior teeth. The presence of third molars should be evaluated. **Lower Left Region:** - Number of teeth: 7- Observation: Includes molars, premolars, and anterior teeth. One tooth appears impacted or unerupted. **Lower Right Region:** - Number of teeth: 6- Observation: Includes molars, premolars, and anterior teeth. One tooth is missing or not visible. **Summary:** The total number of teeth present is 25, with the noted conditions in each quadrant. Further evaluation, such as clinical examination and possibly additional imaging, is recommended to assess impacted or unerupted teeth and any potential pathology.	

Figure 6: Dental Image: Case 1. The task involves quantifying the number of teeth and identifying anomalies in dental X-rays, with critical information highlighted in yellow.

4.2 Medical Report Generation Task Results

As illustrated in **Table 1**, in the zero-shot setting of the MIMIC-CXR dataset, Gemini-1.0-Pro-Vision exhibited strong performance, attaining an R-1 score of 0.2814, an R-2 score of 0.1334, and an R-L score of 0.2259. These metrics notably surpass those achieved by other models operating within similar parameters.

The assessment conducted on the OpenI dataset reveals that the GPT-4o model consistently demonstrates outstanding performance in zero-shot scenarios, achieving R-1 scores of 0.1713, R-2 scores of 0.0622, and R-L scores of 0.1466.

In the zero-shot scenario of the Internal dataset dataset, the GPT-4o model demonstrates robust performance, achieving an R-1 score of 0.2805, an R-2 score of 0.0746, and an R-L score of 0.2635. These results notably outperform those of other models operating under comparable conditions.

In essence, the comparison of Rouge metrics for medical reports generated by various large language models, using identical prompt words and zero-shot techniques, serves as an effective means to gauge the performance discrepancies among these models operating under equivalent conditions. Such evaluation holds considerable importance in guiding the selection of specific task-oriented large language models for future research endeavors and practical applications.

Table 1: Test Results for Compared LLMs. For results within each dataset, each model corresponds to three similarity scores, R-1, R-2, and R-L.

Model	MIMIC-CXR			OpenI			SXY		
	R-1	R-2	R-L	R-1	R-2	R-L	R-1	R-2	R-L
Gemini-1.0-Pro-Vision	0.2814	0.1334	0.2259	0.1654	0.0663	0.1425	0.0103	0.0000	0.0087
Gemini-1.5-Pro	0.1759	0.0624	0.1265	0.1364	0.0505	0.1160	0.0344	0.0124	0.0336
Gemini-1.5-Flash	0.1973	0.0852	0.1488	0.1018	0.0322	0.0811	0.0269	0.0020	0.0250
GPT-3.5-Turbo	0.2406	0.1152	0.1914	0.1529	0.0554	0.1291	0.1010	0.0305	0.0957
GPT-4-Turbo	0.1235	0.0478	0.0925	0.0800	0.0260	0.0647	0.2298	0.0837	0.2173
GPT-4o	0.2275	0.0997	0.1752	0.1713	0.0622	0.1466	0.2805	0.0746	0.2635
Yi-Large	0.0850	0.0346	0.0659	0.0501	0.0153	0.0411	0.2321	0.0968	0.2200
Yi-Large-Turbo	0.1699	0.0728	0.1303	0.0986	0.0329	0.0816	0.1272	0.0518	0.1185
Claude-3-Opus	0.1434	0.0608	0.1080	0.0840	0.0276	0.0704	0.0325	0.0070	0.0299
Llama 3	0.1884	0.0791	0.1429	0.1174	0.0371	0.0971	0.0786	0.0173	0.0740

4.3 Model Generation Time

Given the importance of timeliness in practical applications, our research involved conducting comparative tests on the model’s generation speed using the online platform provided by the model within the same network environment. Specifically, we quantified the total number of characters generated by the model and the time taken for this generation process. Subsequently, we calculated the time required for the model to generate each character, as shown from **Eq. (2)**. As reported in **Fig. 7**, across the five categories of medical image question answering tasks, GPT-4o exhibited the fastest generation speed, except for tasks related to skin image testing. In this particular domain, Gemini-1.0-Pro-Vision demonstrated the fastest performance, with GPT-4o closely following. Gemini-1.5-Pro exhibited the slowest generation speed, with its average time to produce the same number of characters being 9.16 times longer than that of GPT-4o.

$$\text{Character Per Time (ms)} = \frac{\text{Total generation time (ms)}}{\text{Number of characters generated}} \tag{2}$$

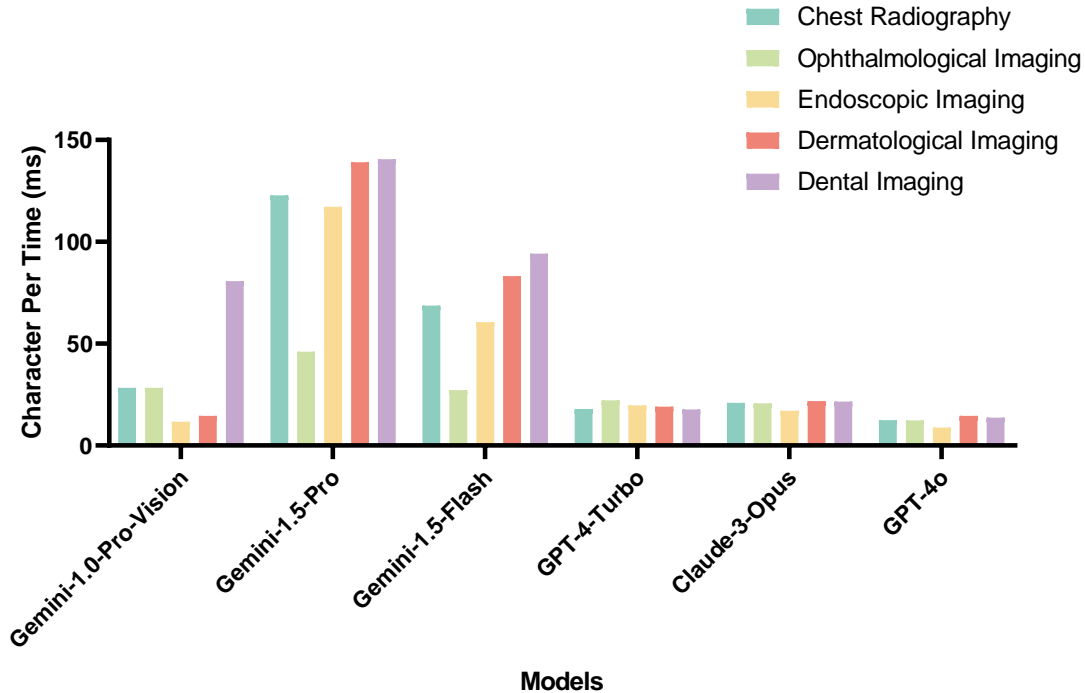


Figure 7: **Comparison of model generation speed.** All comparative tests were conducted under identical network conditions.

5 Discussion and Conclusion

In this comprehensive study, we rigorously evaluated the performance of 10 prominent large models in medical image understanding and radiology report generation, including globally leading models such as Gemini-1.5-Pro, GPT-4o, Claude-3-Opus, Yi-Large-Turbo, among others.

Our assessment benchmarks these models in explaining medical images, summarizing their advantages and disadvantages, and exploring their potential in medical applications. The findings indicate that while current state-of-the-art MLLMs cannot yet be directly applied to the medical field, their robust reasoning abilities and impressive response speed suggest significant potential for improving model generalization in this domain.

Additionally, we benchmarked these models in generating radiological reports to understand their varying capabilities, strengths, and weaknesses. Our results affirm the performance of numerous domestic and international MLLMs, highlighting their untapped potential in healthcare, especially in radiology. These insights indicate a promising development trajectory, with multilingual and diverse MLLMs poised to enhance global healthcare systems.

Looking ahead, our large-scale research provides a foundation for further exploration, suggesting the potential to extend these MLLMs to different medical specialties and develop multimodal medical MLLMs for comprehensive patient health understanding. However, ethical considerations such as privacy protection, model fairness, and interpretability, along with legal and regulatory frameworks, are essential for safe and ethical MLLM deployment in healthcare. In summary, despite the promise of reducing doctors' workloads and alleviating medical resource constraints, significant enhancements and comprehensive validation are urgently needed before clinical deployment of these MLLMs.

References

- [1] Josh Achiam, Steven Adler, Sandhini Agarwal, Lama Ahmad, Ilge Akkaya, Florencia Leoni Aleman, Diogo Almeida, Janko Altschmidt, Sam Altman, Shyamal Anadkat, et al. Gpt-4 technical report. *arXiv preprint arXiv:2303.08774*, 2023.
- [2] AI@Meta. Llama 3 model card. 2024.
- [3] Deepa Anand, Vanika Singhal, Dattesh D Shanbhag, Shriram KS, Uday Patil, Chitresh Bhushan, Kavitha Manickam, Dawei Gui, Rakesh Mullick, Avinash Gopal, et al. One-shot localization and segmentation of medical images with foundation models. *arXiv preprint arXiv:2310.18642*, 2023.
- [4] Rohan Anil, Sebastian Borgeaud, Yonghui Wu, Jean-Baptiste Alayrac, Jiahui Yu, Radu Soricut, Johan Schalkwyk, Andrew M Dai, Anja Hauth, Katie Millican, et al. Gemini: A family of highly capable multimodal models. *arXiv preprint arXiv:2312.11805*, 1, 2023.
- [5] Rohan Anil, Andrew M Dai, Orhan Firat, Melvin Johnson, Dmitry Lepikhin, Alexandre Passos, Siamak Shakeri, Emanuel Taropa, Paige Bailey, Zhifeng Chen, et al. Palm 2 technical report. *arXiv preprint arXiv:2305.10403*, 2023.
- [6] Anthropic. Meet claude: The ai assistant from anthropic. *Anthropic Blog*, 2023.
- [7] Jorge Bernal, F Javier Sánchez, Gloria Fernández-Esparrach, Debora Gil, Cristina Rodríguez, and Fernando Vilariño. Wm-dova maps for accurate polyp highlighting in colonoscopy: Validation vs. saliency maps from physicians. *Computerized medical imaging and graphics*, 43:99–111, 2015.
- [8] Tom Brown, Benjamin Mann, Nick Ryder, Melanie Subbiah, Jared D Kaplan, Prafulla Dhariwal, Arvind Neelakantan, Pranav Shyam, Girish Sastry, Amanda Askell, Sandhini Agarwal, Ariel Herbert-Voss, Gretchen Krueger, Tom Henighan, Rewon Child, Aditya Ramesh, Daniel Ziegler, Jeffrey Wu, Clemens Winter, Chris Hesse, Mark Chen, Eric Sigler, Mateusz Litwin, Scott Gray, Benjamin Chess, Jack Clark, Christopher Berner, Sam McCandlish, Alec Radford, Ilya Sutskever, and Dario Amodei. Language models are few-shot learners. In H. Larochelle, M. Ranzato, R. Hadsell, M.F. Balcan, and H. Lin, editors, *Advances in Neural Information Processing Systems*, volume 33, pages 1877–1901. Curran Associates, Inc., 2020.
- [9] Tom Brown, Benjamin Mann, Nick Ryder, Melanie Subbiah, Jared D Kaplan, Prafulla Dhariwal, Arvind Neelakantan, Pranav Shyam, Girish Sastry, Amanda Askell, et al. Language models are few-shot learners. *Advances in neural information processing systems*, 33:1877–1901, 2020.
- [10] Yupeng Chang, Xu Wang, Jindong Wang, Yuan Wu, Linyi Yang, Kaijie Zhu, Hao Chen, Xiaoyuan Yi, Cunxiang Wang, Yidong Wang, et al. A survey on evaluation of large language models. *ACM Transactions on Intelligent Systems and Technology*, 15(3):1–45, 2024.
- [11] Soravit Changpinyo, Piyush Sharma, Nan Ding, and Radu Soricut. Conceptual 12m: Pushing web-scale image-text pre-training to recognize long-tail visual concepts. In *CVPR*, 2021.
- [12] Chi Chen, Ruoyu Qin, Fuwen Luo, Xiaoyue Mi, Peng Li, Maosong Sun, and Yang Liu. Position-enhanced visual instruction tuning for multimodal large language models. *arXiv preprint arXiv:2308.13437*, 2023.
- [13] Gaole H Chen, Shizhe Chen, Renrui Zhang, Jiawei Chen, Xiaoyu Wu, Zhou Zhang, Zecheng

-
- Chen, Jinfeng Li, Xing Wan, and Bin Wang. Allava: Harnessing gpt4v-synthesized data for a lite vision-language model. *arXiv preprint arXiv:2402.11684*, 2024.
- [14] Yukang Chen, Shengju Qian, Haotian Tang, Xin Lai, Zhijian Liu, Song Han, and Jiaya Jia. Longlora: Efficient fine-tuning of long-context large language models. *arXiv preprint arXiv:2309.12307*, 2023.
- [15] Inyoung Cheong, King Xia, K. J. Kevin Feng, Quan Ze Chen, and Amy X. Zhang. (a)i am not a lawyer, but...: Engaging legal experts towards responsible llm policies for legal advice. In *Proceedings of the 2024 ACM Conference on Fairness, Accountability, and Transparency, FAccT '24*, page 2454–2469, New York, NY, USA, 2024. Association for Computing Machinery.
- [16] Aakanksha Chowdhery, Sharan Narang, Jacob Devlin, Maarten Bosma, Gaurav Mishra, Adam Roberts, Paul Barham, Hyung Won Chung, Charles Sutton, Sebastian Gehrmann, et al. Palm: Scaling language modeling with pathways. *Journal of Machine Learning Research*, 24(240):1–113, 2023.
- [17] Muhammad E. H. Chowdhury, Tawsifur Rahman, Amith Khandakar, Rashid Mazhar, Muhammad Abdul Kadir, Zaid Bin Mahbub, Khandakar Reajul Islam, Muhammad Salman Khan, Atif Iqbal, Nasser Al Emadi, Mamun Bin Ibne Reaz, and Mohammad Tariqul Islam. Can ai help in screening viral and covid-19 pneumonia? *IEEE Access*, 8:132665–132676, 2020.
- [18] Hyung Won Chung, Le Hou, Shayne Longpre, Barret Zoph, Yi Tay, William Fedus, Yunxuan Li, Xuezhi Wang, Mostafa Dehghani, Siddhartha Brahma, et al. Scaling instruction-finetuned language models. *arXiv preprint arXiv:2210.11416*, 2022.
- [19] Jiayi Cui, Zongjian Li, Yang Yan, Bohua Chen, and Li Yuan. Chatlaw: Open-source legal large language model with integrated external knowledge bases. *arXiv preprint arXiv:2306.16092*, 2023.
- [20] Aysen Degerli, Mete Ahishali, Mehmet Yamac, Serkan Kiranyaz, Muhammad EH Chowdhury, Khalid Hameed, Tahir Hamid, Rashid Mazhar, and Moncef Gabbouj. Covid-19 infection map generation and detection from chest x-ray images. *Health information science and systems*, 9(1):15, 2021.
- [21] Jacob Devlin, Ming-Wei Chang, Kenton Lee, and Kristina Toutanova. Bert: Pre-training of deep bidirectional transformers for language understanding. *arXiv preprint arXiv:1810.04805*, 2018.
- [22] Zhengxiao Du, Yujie Qian, Xiao Liu, Ming Ding, Jiezhong Qiu, Zhilin Yang, and Jie Tang. Glm: General language model pretraining with autoregressive blank infilling. *arXiv preprint arXiv:2103.10360*, 2021.
- [23] Luciano Floridi and Massimo Chiriatti. Gpt-3: Its nature, scope, limits, and consequences. *Minds and Machines*, 30:681–694, 2020.
- [24] Chaoyou Fu, Pengbo Chen, Yi Shen, Yixiang Qin, Min Zhang, Xiaoqi Lin, Zhenyu Qiu, Weihang Lin, Zhenling Qiu, Wenjing Lin, et al. Mme: A comprehensive evaluation benchmark for multimodal large language models. In *arXiv preprint arXiv:2306.13394*, 2023.
- [25] Yingqiang Ge, Wenyue Hua, Kai Mei, Jianchao Ji, Juntao Tan, Shuyuan Xu, Zelong Li, and Yongfeng Zhang. Openagi: When llm meets domain experts. In A. Oh, T. Naumann, A. Globerson, K. Saenko, M. Hardt, and S. Levine, editors, *Advances in Neural Information Processing Systems*, volume 36, pages 5539–5568. Curran Associates, Inc., 2023.
-

-
- [26] Zishan Guo, Renren Jin, Chuang Liu, Yufei Huang, Dan Shi, Linhao Yu, Yan Liu, Jiaxuan Li, Bojian Xiong, Deyi Xiong, et al. Evaluating large language models: A comprehensive survey. *arXiv preprint arXiv:2310.19736*, 2023.
- [27] Xu Han, Zhengyan Zhang, Ning Ding, Yuxian Gu, Xiao Liu, Yuqi Huo, Jiezhong Qiu, Yuan Yao, Ao Zhang, Liang Zhang, et al. Pre-trained models: Past, present and future. *AI Open*, 2:225–250, 2021.
- [28] Sameera Horawalavithana, Sai Munikoti, Ian Stewart, and Henry Kvinge. Scitune: Aligning large language models with scientific multimodal instructions. *arXiv preprint arXiv:2307.01139*, 2023.
- [29] Muhammad Irfan and LIAM MURRAY. Micro- Credential: A guide to prompt writing and engineering in higher education: A tool for Artificial Intelligence in LLM. 5 2023.
- [30] Ahmed Izzidien, Holli Sargeant, and Felix Steffek. Llm vs. lawyers: Identifying a subset of summary judgments in a large uk case law dataset. *arXiv preprint arXiv:2403.04791*, 2024.
- [31] Jongseong Jang, Daeun Kyung, Seung Hwan Kim, Honglak Lee, Kyunghoon Bae, and Edward Choi. Significantly improving zero-shot x-ray pathology classification via fine-tuning pre-trained image-text encoders. *arXiv preprint arXiv:2212.07050*, 2022.
- [32] Debesh Jha, Pia H Smedsrud, Michael A Riegler, Pål Halvorsen, Thomas de Lange, Dag Johansen, and Håvard D Johansen. Kvasir-seg: A segmented polyp dataset. In *International Conference on Multimedia Modeling*, pages 451–462. Springer, 2020.
- [33] Alistair Johnson, Tom Pollard, Roger Mark, Seth Berkowitz, and Steven Horng. Mimic-cxr database. *PhysioNet10*, 13026:C2JT1Q.
- [34] Matthias Keicher, Kamilia Zaripova, Tobias Czempiel, Kristina Mach, Ashkan Khakzar, and Nassir Navab. Flexr: Few-shot classification with language embeddings for structured reporting of chest x-rays. In *Medical Imaging with Deep Learning*, pages 1493–1508. PMLR, 2024.
- [35] Daniel Kermany, Kang Zhang, Michael Goldbaum, et al. Labeled optical coherence tomography (oct) and chest x-ray images for classification. *Mendeley data*, 2(2):651, 2018.
- [36] Alexander Kirillov, Eric Mintun, Nikhila Ravi, Hanzi Mao, Chloe Rolland, Laura Gustafson, Tete Xiao, Saeid Whitehead, Alexander C Berg, Wan-Yen Lo, et al. Segment anything. In *arXiv preprint arXiv:2304.02643*, 2023.
- [37] Zhenzhong Lan, Mingda Chen, Sebastian Goodman, Kevin Gimpel, Piyush Sharma, and Radu Soricut. Albert: A lite bert for self-supervised learning of language representations. *arXiv preprint arXiv:1909.11942*, 2019.
- [38] Gyeong-Geon Lee, Lehong Shi, Ehsan Latif, Yizhu Gao, Arne Bewersdorf, Matthew Nyaaba, Shuchen Guo, Zihao Wu, Zhengliang Liu, Hui Wang, et al. Multimodality of ai for education: Towards artificial general intelligence. *arXiv preprint arXiv:2312.06037*, 2023.
- [39] Mike Lewis, Yinhan Liu, Naman Goyal, Marjan Ghazvininejad, Abdelrahman Mohamed, Omer Levy, Ves Stoyanov, and Luke Zettlemoyer. Bart: Denoising sequence-to-sequence pre-training for natural language generation, translation, and comprehension. *arXiv preprint arXiv:1910.13461*, 2019.
- [40] Junnan Li, Dongxu Li, Silvio Savarese, and Steven Hoi. Blip-2: Bootstrapping language-image
-

-
- pre-training with frozen image encoders and large language models. In *International conference on machine learning*, pages 19730–19742. PMLR, 2023.
- [41] Chin-Yew Lin. Rouge: A package for automatic evaluation of summaries. In *Text summarization branches out*, pages 74–81, 2004.
- [42] Weixiong Lin, Ziheng Zhao, Xiaoman Zhang, Chaoyi Wu, Ya Zhang, Yanfeng Wang, and Weidi Xie. Pmc-clip: Contrastive language-image pre-training using biomedical documents. In *International Conference on Medical Image Computing and Computer-Assisted Intervention*, pages 525–536. Springer, 2023.
- [43] Haotian Liu, Chunyuan Li, Qingyang Wu, and Yong Jae Lee. Visual instruction tuning. In *arXiv preprint arXiv:2304.08485*, 2023.
- [44] Haotian Liu, Chunyuan Li, Qingyang Wu, and Yong Jae Lee. Visual instruction tuning. *Advances in neural information processing systems*, 36, 2024.
- [45] Jie Liu, Yixiao Zhang, Jie-Neng Chen, Junfei Xiao, Yongyi Lu, Bennett A Landman, Yixuan Yuan, Alan Yuille, Yucheng Tang, and Zongwei Zhou. Clip-driven universal model for organ segmentation and tumor detection. In *Proceedings of the IEEE/CVF International Conference on Computer Vision*, pages 21152–21164, 2023.
- [46] Pengfei Liu, Weizhe Yuan, Jinlan Fu, Zhengbao Jiang, Hiroaki Hayashi, and Graham Neubig. Pre-train, prompt, and predict: A systematic survey of prompting methods in natural language processing. *ACM Computing Surveys*, 55(9):1–35, 2023.
- [47] Yang Liu, Huiwen Duan, Yuyang Zhang, Bohan Li, Songlin Zhang, Wei Zhao, Ye Yuan, Jiajun Wang, Cheng He, Ziwei Liu, et al. Mmbench: Is your multi-modal model an all-around player? In *arXiv preprint arXiv:2307.06281*, 2023.
- [48] Yiheng Liu, Tianle Han, Siyuan Ma, Jiayue Zhang, Yuanyuan Yang, Jiaming Tian, Hao He, Antong Li, Mengshen He, Zhengliang Liu, Zihao Wu, Lin Zhao, Dajiang Zhu, Xiang Li, Ning Qiang, Dingang Shen, Tianming Liu, and Bao Ge. Summary of chatgpt-related research and perspective towards the future of large language models. *Meta-Radiology*, 1(2):100017, 2023.
- [49] Yinhan Liu, Myle Ott, Naman Goyal, Jingfei Du, Mandar Joshi, Danqi Chen, Omer Levy, Mike Lewis, Luke Zettlemoyer, and Veselin Stoyanov. Roberta: A robustly optimized bert pretraining approach. *arXiv preprint arXiv:1907.11692*, 2019.
- [50] Ze Liu, Yutong Lin, Yue Cao, Han Hu, Yixuan Wei, Zheng Zhang, Stephen Lin, and Baining Guo. Swin transformer: Hierarchical vision transformer using shifted windows. In *Proceedings of the IEEE/CVF international conference on computer vision*, pages 10012–10022, 2021.
- [51] Zhengliang Liu, Lu Zhang, Zihao Wu, Xiaowei Yu, Chao Cao, Haixing Dai, Ninghao Liu, Jun Liu, Wei Liu, Quanzheng Li, et al. Surviving chatgpt in healthcare. *Frontiers in Radiology*, 3:1224682, 2024.
- [52] Zhengliang Liu, Tianyang Zhong, Yiwei Li, Yutong Zhang, Yi Pan, Zihao Zhao, Peixin Dong, Chao Cao, Yuxiao Liu, Peng Shu, et al. Evaluating large language models for radiology natural language processing. *arXiv preprint arXiv:2307.13693*, 2023.
- [53] Zhengliang Liu, Tianyang Zhong, Yiwei Li, Yutong Zhang, Yi Pan, Zihao Zhao, Peixin Dong, Chao Cao, Yuxiao Liu, Peng Shu, Yaonai Wei, Zihao Wu, Chong Ma, Jiaqi Wang, Sheng Wang, Mengyue Zhou, Zuwei Jiang, Chunlin Li, Jason Holmes, Shaochen Xu, Lu Zhang, Haixing
-

-
- Dai, Kai Zhang, Lin Zhao, Yuanhao Chen, Xu Liu, Peilong Wang, Pingkun Yan, Jun Liu, Bao Ge, Lichao Sun, Dajiang Zhu, Xiang Li, Wei Liu, Xiaoyan Cai, Xintao Hu, Xi Jiang, Shu Zhang, Xin Zhang, Tuo Zhang, Shijie Zhao, Quanzheng Li, Hongtu Zhu, Dinggang Shen, and Tianming Liu. Evaluating large language models for radiology natural language processing, 2023.
- [54] Yadong Lu, Chunyuan Li, Haotian Liu, Jianwei Yang, Jianfeng Gao, and Yelong Shen. An empirical study of scaling instruct-tuned large multimodal models. *arXiv preprint arXiv:2309.09958*, 2023.
- [55] Renqian Luo, Liai Sun, Yingce Xia, Tao Qin, Sheng Zhang, Hoifung Poon, and Tie-Yan Liu. Biogpt: generative pre-trained transformer for biomedical text generation and mining. *Briefings in bioinformatics*, 23(6):bbac409, 2022.
- [56] Chong Ma, Zihao Wu, Jiaqi Wang, Shaochen Xu, Yaonai Wei, Zhengliang Liu, Fang Zeng, Xi Jiang, Lei Guo, Xiaoyan Cai, Shu Zhang, Tuo Zhang, Dajiang Zhu, Dinggang Shen, Tianming Liu, and Xiang Li. An iterative optimizing framework for radiology report summarization with chatgpt. *IEEE Transactions on Artificial Intelligence*, pages 1–12, 2024.
- [57] Salman Maqbool, Aqsa Riaz, Hasan Sajid, and Osman Hasan. m2caiseg: Semantic segmentation of laparoscopic images using convolutional neural networks. *arXiv preprint arXiv:2008.10134*, 2020.
- [58] Aakash Mishra, Rajat Mittal, Christy Jestin, Kostas Tingos, and Pranav Rajpurkar. Improving zero-shot detection of low prevalence chest pathologies using domain pre-trained language models. *arXiv preprint arXiv:2306.08000*, 2023.
- [59] Michael Moor, Oishi Banerjee, Zahra Shakeri Hossein Abad, Harlan M Krumholz, Jure Leskovec, Eric J Topol, and Pranav Rajpurkar. Foundation models for generalist medical artificial intelligence. *Nature*, 616(7956):259–265, 2023.
- [60] Steven Moore, Richard Tong, Anjali Singh, Zitao Liu, Xianguen Hu, Yu Lu, Joleen Liang, Chen Cao, Hassan Khosravi, Paul Denny, Chris Brooks, and John Stamper. Empowering education with llms - the next-gen interface and content generation. In Ning Wang, Genaro Rebolledo-Mendez, Vania Dimitrova, Noboru Matsuda, and Olga C. Santos, editors, *Artificial Intelligence in Education. Posters and Late Breaking Results, Workshops and Tutorials, Industry and Innovation Tracks, Practitioners, Doctoral Consortium and Blue Sky*, pages 32–37, Cham, 2023. Springer Nature Switzerland.
- [61] OpenAI. Gpt-4 technical report. *arXiv preprint arXiv:2303.08774*, 2023.
- [62] Maxime Oquab, Thomas Darcet, Timothee Moutakanni, Huy Vo, Marc Szafraniec, Vasil Khalidov, Pierre Fernandez, Daniel Haziza, Francisco Massa, Alaaeldin El-Nouby, et al. Dinov2: Learning robust visual features without supervision. *arXiv preprint arXiv:2304.07193*, 2023.
- [63] Long Ouyang, Jeffrey Wu, Xu Jiang, Diogo Almeida, Carroll Wainwright, Pamela Mishkin, Chong Zhang, Sandhini Agarwal, Katarina Slama, Alex Ray, et al. Training language models to follow instructions with human feedback. *Advances in neural information processing systems*, 35:27730–27744, 2022.
- [64] Long Ouyang, Jeffrey Wu, Xu Jiang, Diogo Almeida, Carroll Wainwright, Pamela Mishkin, Chong Zhang, Sandhini Agarwal, Katarina Slama, Alex Ray, John Schulman, Jacob Hilton,
-

-
- Fraser Kelton, Luke Miller, Maddie Simens, Amanda Askill, Peter Welinder, Paul F Christiano, Jan Leike, and Ryan Lowe. Training language models to follow instructions with human feedback. In S. Koyejo, S. Mohamed, A. Agarwal, D. Belgrave, K. Cho, and A. Oh, editors, *Advances in Neural Information Processing Systems*, volume 35, pages 27730–27744. Curran Associates, Inc., 2022.
- [65] Chantal Pellegrini, Matthias Keicher, Ege Özsoy, Petra Jiraskova, Rickmer Braren, and Nassir Navab. Xplainer: From x-ray observations to explainable zero-shot diagnosis. In *International Conference on Medical Image Computing and Computer-Assisted Intervention*, pages 420–429. Springer, 2023.
- [66] Baolin Peng, Chunyuan Li, Pengcheng He, Michel Galley, and Jianfeng Gao. Instruction tuning with gpt-4. *arXiv preprint arXiv:2304.03277*, 2023.
- [67] Baolin Peng, Chunyuan Li, Zirui Lin, Wei Zhang, Yiping Jiang, Lianhui Zhou, Yiwen Sheng, Xian Wang, Yong Gao, Daxin Jiang, Pengcheng He, et al. Kosmos-1: Simulating human-like compositionality and concept learning. *arXiv preprint arXiv:2306.14828*, 2023.
- [68] Kanchan Poudel, Manish Dhakal, Prasiddha Bhandari, Rabin Adhikari, Safal Thapaliya, and Bishesh Khanal. Exploring transfer learning in medical image segmentation using vision-language models. *arXiv preprint arXiv:2308.07706*, 2023.
- [69] Alec Radford, Jong Wook Kim, Chris Hallacy, Aditya Ramesh, Gabriel Goh, Sandhini Agarwal, Girish Sastry, Amanda Askill, Pamela Mishkin, Jack Clark, et al. Learning transferable visual models from natural language supervision. In *International conference on machine learning*, pages 8748–8763. PMLR, 2021.
- [70] Alec Radford, Jeffrey Wu, Rewon Child, David Luan, Dario Amodei, Ilya Sutskever, et al. Language models are unsupervised multitask learners. *OpenAI blog*, 1(8):9, 2019.
- [71] Colin Raffel, Noam Shazeer, Adam Roberts, Katherine Lee, Sharan Narang, Michael Matena, Yanqi Zhou, Wei Li, and Peter J. Liu. Exploring the limits of transfer learning with a unified text-to-text transformer. *Journal of Machine Learning Research*, 21(140):1–67, 2020.
- [72] Colin Raffel, Noam Shazeer, Adam Roberts, Katherine Lee, Sharan Narang, Michael Matena, Yanqi Zhou, Wei Li, and Peter J Liu. Exploring the limits of transfer learning with a unified text-to-text transformer. *Journal of machine learning research*, 21(140):1–67, 2020.
- [73] Tawsifur Rahman, Amith Khandakar, Yazan Qiblawey, Anas Tahir, Serkan Kiranyaz, Saad Bin Abul Kashem, Mohammad Tariqul Islam, Somaya Al Maadeed, Susu M. Zughaiyer, Muhammad Salman Khan, and Muhammad E.H. Chowdhury. Exploring the effect of image enhancement techniques on covid-19 detection using chest x-ray images. *Computers in Biology and Medicine*, 132:104319, 2021.
- [74] Robin Rombach, Andreas Blattmann, Dominik Lorenz, Patrick Esser, and Björn Ommer. High-resolution image synthesis with latent diffusion models. In *Proceedings of the IEEE/CVF conference on computer vision and pattern recognition*, pages 10684–10695, 2022.
- [75] V. Rotemberg, N. Kurtansky, B. Betz-Stablein, L. Caffery, E. Chousakos, N. Codella, M. Combalia, S. Dusza, P. Guitera, D. Gutman, A. Halpern, B. Helba, H. Kittler, K. Kose, S. Langer, K. Lioprys, J. Malvey, S. Musthaq, J. Nanda, O. Reiter, G. Shih, A. Stratigos, P. Tschandl, J. Weber, and P. Soyer. A patient-centric dataset of images and metadata for identifying melanomas using clinical context. *Sci Data*, 8(34):1–15, 2021.
-

-
- [76] Khaled Saab, Tao Tu, Wei-Hung Weng, Ryutaro Tanno, David Stutz, Ellery Wulczyn, Fan Zhang, Tim Strother, Chunjong Park, Elahe Vedadi, et al. Capabilities of gemini models in medicine. *arXiv preprint arXiv:2404.18416*, 2024.
- [77] Christoph Schuhmann, Richard Beaumont, Romain Vencu, Cade Gordon, Ross Wightman, Mehdi Cherti, Timothy Coombes, Aarush Katta, Clayton Mullis, Mitchell Wortsman, et al. Laion-5b: An open large-scale dataset for training next generation image-text models. In *NeurIPS*, 2022.
- [78] Piyush Sharma, Nan Ding, Sebastian Goodman, and Radu Soricut. Conceptual captions: A cleaned, hypernymed, image alt-text dataset for automatic image captioning. In *ACL*, 2018.
- [79] Yu Shen, Chaoyou Fu, Pengbo Chen, Min Zhang, Keyi Li, Xuejing Sun, Yi Wu, Shu Lin, and Rongrong Ji. Aligning and prompting everything all at once for universal visual perception. In *CVPR*, 2024.
- [80] Peilun Shi, Jianing Qiu, Sai Mu Dalike Abaxi, Hao Wei, Frank P-W Lo, and Wu Yuan. Generalist vision foundation models for medical imaging: A case study of segment anything model on zero-shot medical segmentation. *Diagnostics*, 13(11):1947, 2023.
- [81] Peng Shu, Huaqin Zhao, Hanqi Jiang, Yiwei Li, Shaochen Xu, Yi Pan, Zihao Wu, Zhengliang Liu, Guoyu Lu, Le Guan, et al. Llms for coding and robotics education. *arXiv preprint arXiv:2402.06116*, 2024.
- [82] K. Singhal, T. Tu, J. Gottweis, et al. Towards expert-level medical question answering with large language models. *arXiv preprint arXiv:2305.09617*, 2023.
- [83] Zhiying Sun, Sheng Shen, Siqi Cao, Haotian Liu, Chunyuan Li, Yujun Shen, Chuang Gan, Li-Yen Gui, Yen-Xiang Wang, Yinan Yang, et al. Aligning large multimodal models with factually augmented rlhf. In *arXiv preprint arXiv:2309.14525*, 2023.
- [84] Anas M. Tahir, Muhammad E.H. Chowdhury, Amith Khandakar, Tawsifur Rahman, Yazan Qiblawey, Uzair Khurshid, Serkan Kiranyaz, Nabil Ibtehaz, M. Sohel Rahman, Somaya Al-Maadeed, Sakib Mahmud, Maymouna Ezeddin, Khaled Hameed, and Tahir Hamid. Covid-19 infection localization and severity grading from chest x-ray images. *Computers in Biology and Medicine*, 139:105002, 2021.
- [85] Yi Tay, Mostafa Dehghani, Vinh Q Tran, Xavier Garcia, Jason Wei, Xuezhi Wang, Hyung Won Chung, Siamak Shakeri, Dara Bahri, Tal Schuster, et al. Ul2: Unifying language learning paradigms. *arXiv preprint arXiv:2205.05131*, 2022.
- [86] Christo Kurisummoottil Thomas, Christina Chaccour, Walid Saad, Mérouane Debbah, and Choong Seon Hong. Causal reasoning: Charting a revolutionary course for next-generation ai-native wireless networks. *IEEE Vehicular Technology Magazine*, 2024.
- [87] Ekin Tiu, Ellie Talius, Pujan Patel, Curtis P Langlotz, Andrew Y Ng, and Pranav Rajpurkar. Expert-level detection of pathologies from unannotated chest x-ray images via self-supervised learning. *Nature Biomedical Engineering*, 6(12):1399–1406, 2022.
- [88] Hugo Touvron, Thibaut Lavril, Gautier Izacard, Xavier Martinet, Marie-Anne Lachaux, Timothée Lacroix, Baptiste Rozière, Naman Goyal, Eric Hambro, Faisal Azhar, et al. Llama: Open and efficient foundation language models. *arXiv preprint arXiv:2302.13971*, 2023.
-

-
- [89] Hugo Touvron, Louis Martin, Kevin Stone, Peter Albert, Amjad Almahairi, Yasmine Babaei, Nikolay Bashlykov, Soumya Batra, Prajwal Bhargava, Shruti Bhosale, et al. Llama 2: Open foundation and fine-tuned chat models. *arXiv preprint arXiv:2307.09288*, 2023.
- [90] Philipp Tschandl. The HAM10000 dataset, a large collection of multi-source dermatoscopic images of common pigmented skin lesions, 2018.
- [91] Andru P Twinanda, Sherif Shehata, Didier Mutter, Jacques Marescaux, Michel De Mathelin, and Nicolas Padoy. Endonet: a deep architecture for recognition tasks on laparoscopic videos. *IEEE transactions on medical imaging*, 36(1):86–97, 2016.
- [92] Tom van Sonsbeek and Marcel Worring. X-tra: Improving chest x-ray tasks with cross-modal retrieval augmentation. In *International Conference on Information Processing in Medical Imaging*, pages 471–482. Springer, 2023.
- [93] Ashish Vaswani, Noam Shazeer, Niki Parmar, Jakob Uszkoreit, Llion Jones, Aidan N Gomez, Lukasz Kaiser, and Illia Polosukhin. Attention is all you need. *Advances in neural information processing systems*, 30, 2017.
- [94] Chenglong Wang, Hang Zhou, Kaiyan Chang, Tongran Liu, Chunliang Zhang, Quan Du, Tong Xiao, and Jingbo Zhu. Learning evaluation models from large language models for sequence generation. *arXiv preprint arXiv:2308.04386*, 2023.
- [95] Jiaqi Wang, Zhengliang Liu, Lin Zhao, Zihao Wu, Chong Ma, Sigang Yu, Haixing Dai, Qiushi Yang, Yiheng Liu, Songyao Zhang, Enze Shi, Yi Pan, Tuo Zhang, Dajiang Zhu, Xiang Li, Xi Jiang, Bao Ge, Yixuan Yuan, Dinggang Shen, Tianming Liu, and Shu Zhang. Review of large vision models and visual prompt engineering. *Meta-Radiology*, 1(3):100047, 2023.
- [96] Thomas Wang, Adam Roberts, Daniel Hesslow, Teven Le Scao, Hyung Won Chung, Iz Beltagy, Julien Launay, and Colin Raffel. What language model architecture and pretraining objective works best for zero-shot generalization? In *International Conference on Machine Learning*, pages 22964–22984. PMLR, 2022.
- [97] Yaqing Wang, Jialin Wu, Tanmaya Dabral, Jiageng Zhang, Geoff Brown, Chun-Ta Lu, Frederick Liu, Yi Liang, Bo Pang, Michael Bendersky, et al. Non-intrusive adaptation: Input-centric parameter-efficient fine-tuning for versatile multimodal modeling. *arXiv preprint arXiv:2310.12100*, 2023.
- [98] Yiqi Wang, Wentao Chen, Xiaotian Han, Xudong Lin, Haiteng Zhao, Yongfei Liu, Bohan Zhai, Jianbo Yuan, Quanzeng You, and Hongxia Yang. Exploring the reasoning abilities of multimodal large language models (mllms): A comprehensive survey on emerging trends in multimodal reasoning. *arXiv preprint arXiv:2401.06805*, 2024.
- [99] Zifeng Wang, Zhenbang Wu, Dinesh Agarwal, and Jimeng Sun. Medclip: Contrastive learning from unpaired medical images and text. *arXiv preprint arXiv:2210.10163*, 2022.
- [100] Jason Wei, Yi Tay, Rishi Bommasani, Colin Raffel, Barret Zoph, Sebastian Borgeaud, Dani Yogatama, Maarten Bosma, Denny Zhou, Donald Metzler, et al. Emergent abilities of large language models. *arXiv preprint arXiv:2206.07682*, 2022.
- [101] Jason Wei, Xuezhi Wang, Dale Schuurmans, Maarten Bosma, Fei Xia, Ed Chi, Quoc V Le, Denny Zhou, et al. Chain-of-thought prompting elicits reasoning in large language models. *Advances in neural information processing systems*, 35:24824–24837, 2022.
-

-
- [102] Lirong Wen, Xuedong Yang, Dongyi Fu, Xinlong Wang, Peixian Cai, Xin Li, Tao Ma, Yayun Li, Lebin Xu, Dapeng Shang, et al. On the road with gpt-4v (ision): Early explorations of visual-language model on autonomous driving. In *arXiv preprint arXiv:2311.05332*, 2023.
- [103] Anton Wiehe, Florian Schneider, Sebastian Blank, Xintong Wang, Hans-Peter Zorn, and Chris Biemann. Language over labels: Contrastive language supervision exceeds purely label-supervised classification performance on chest x-rays. In *Proceedings of the 2nd Conference of the Asia-Pacific Chapter of the Association for Computational Linguistics and the 12th International Joint Conference on Natural Language Processing: Student Research Workshop*, pages 76–83, 2022.
- [104] Honglin Xiong, Sheng Wang, Yitao Zhu, Zihao Zhao, Yuxiao Liu, Qian Wang, and Dinggang Shen. Doctorglm: Fine-tuning your chinese doctor is not a herculean task. *arXiv preprint arXiv:2304.01097*, 2023.
- [105] Runxin Xu, Fuli Luo, Zhiyuan Zhang, Chuanqi Tan, Baobao Chang, Songfang Huang, and Fei Huang. Raise a child in large language model: Towards effective and generalizable fine-tuning. *arXiv preprint arXiv:2109.05687*, 2021.
- [106] Hao Yang, Junyang Lin, An Yang, Peng Wang, Chang Zhou, and Hongxia Yang. Prompt tuning for generative multimodal pretrained models. *arXiv preprint arXiv:2208.02532*, 2022.
- [107] Jingfeng Yang, Hongye Jin, Ruixiang Tang, Xiaotian Han, Qizhang Feng, Haoming Jiang, Bing Yin, and Xia Hu. Harnessing the power of llms in practice: A survey on chatgpt and beyond. 2023.
- [108] Zekun Yang, Linxi Li, Kevin Lin, Jing Wang, Chung-Cheng Lin, Zicheng Liu, and Lin Wang. The dawn of lmms: Preliminary explorations with gpt-4v (ision). In *arXiv preprint arXiv:2309.17421*, 2023.
- [109] Shukang Yin, Chaoyou Fu, Sirui Zhao, Ke Li, Xing Sun, Tong Xu, and Enhong Chen. A survey on multimodal large language models. *IEEE Transactions on Pattern Analysis and Machine Intelligence*, 2023.
- [110] Tao Yu, Yue Yao, Hang Zhang, Tianxiang He, Yizhuo Han, Ge Cui, Jiarong Hu, Zhenfeng Liu, Hua-Tong Zheng, Maosong Sun, et al. Rlhf-v: Towards trustworthy mllms via behavior alignment from fine-grained correctional human feedback. In *arXiv preprint arXiv:2312.00849*, 2023.
- [111] Wenhai Yu, Zhe Yang, Linxi Li, Jing Wang, Kevin Lin, Zicheng Liu, Xin Wang, and Lin Wang. Mm-vet: Evaluating large multimodal models for integrated capabilities. In *arXiv preprint arXiv:2308.02490*, 2023.
- [112] Yuexiang Zhai, Shengbang Tong, Xiao Li, Mu Cai, Qing Qu, Yong Jae Lee, and Yi Ma. Investigating the catastrophic forgetting in multimodal large language models. *arXiv preprint arXiv:2309.10313*, 2023.
- [113] Hao Zhang, Feng Li, Shilong Liu, Lei Zhang, Hang Su, Jun Zhu, Lionel M Ni, and Heung-Yeung Shum. Dino: Detr with improved denoising anchor boxes for end-to-end object detection. *arXiv preprint arXiv:2203.03605*, 2022.
- [114] Hao Zhang, Wenqi Shao, Hong Liu, Yongqiang Ma, Ping Luo, Yu Qiao, and Kaipeng Zhang. Avibench: Towards evaluating the robustness of large vision-language model on adversarial visual-instructions. *arXiv preprint arXiv:2403.09346*, 2024.
-

-
- [115] Lian Zhang, Zhengliang Liu, Lu Zhang, Zihao Wu, Xiaowei Yu, Jason Holmes, Hongying Feng, Haixing Dai, Xiang Li, Quanzheng Li, et al. Generalizable and promptable artificial intelligence model to augment clinical delineation in radiation oncology. *Medical physics*, 51(3):2187–2199, 2024.
- [116] Sheng Zhang, Yanbo Xu, Naoto Usuyama, Hanwen Xu, Jaspreet Bagga, Robert Tinn, Sam Preston, Rajesh Rao, Mu Wei, Naveen Valluri, et al. Biomedclip: a multimodal biomedical foundation model pretrained from fifteen million scientific image-text pairs. *arXiv preprint arXiv:2303.00915*, 2023.
- [117] Susan Zhang, Stephen Roller, Naman Goyal, Mikel Artetxe, Moya Chen, Shuohui Chen, Christopher Dewan, Mona Diab, Xian Li, Xi Victoria Lin, et al. Opt: Open pre-trained transformer language models. *arXiv preprint arXiv:2205.01068*, 2022.
- [118] Haiyan Zhao, Hanjie Chen, Fan Yang, Ninghao Liu, Huiqi Deng, Hengyi Cai, Shuaiqiang Wang, Dawei Yin, and Mengnan Du. Explainability for large language models: A survey. *ACM Transactions on Intelligent Systems and Technology*, 15(2):1–38, 2024.
- [119] Huan Zhao, Qian Ling, Yi Pan, Tianyang Zhong, Jin-Yu Hu, Junjie Yao, Fengqian Xiao, Zhenxiang Xiao, Yutong Zhang, San-Hua Xu, et al. Ophtha-llama2: A large language model for ophthalmology. *arXiv preprint arXiv:2312.04906*, 2023.
- [120] Wayne Xin Zhao, Kun Zhou, Junyi Li, Tianyi Tang, Xiaolei Wang, Yupeng Hou, Yingqian Min, Beichen Zhang, Junjie Zhang, Zican Dong, et al. A survey of large language models. *arXiv preprint arXiv:2303.18223*, 2023.
- [121] Zihao Zhao, Sheng Wang, Jinchen Gu, Yitao Zhu, Lanzhuju Mei, Zixu Zhuang, Zhiming Cui, Qian Wang, and Dinggang Shen. Chatcad+: Towards a universal and reliable interactive cad using llms. *arXiv preprint arXiv:2305.15964*, 2023.
- [122] Tianyang Zhong, Wei Zhao, Yutong Zhang, Yi Pan, Peixin Dong, Zuowei Jiang, Xiaoyan Kui, Youlan Shang, Li Yang, Yaonai Wei, et al. Chatradio-valuer: a chat large language model for generalizable radiology report generation based on multi-institution and multi-system data. *arXiv preprint arXiv:2310.05242*, 2023.
- [123] Tianyang Zhong, Wei Zhao, Yutong Zhang, Yi Pan, Peixin Dong, Zuowei Jiang, Xiaoyan Kui, Youlan Shang, Li Yang, Yaonai Wei, Longtao Yang, Hao Chen, Huan Zhao, Yuxiao Liu, Ning Zhu, Yiwei Li, Yisong Wang, Jiaqi Yao, Jiaqi Wang, Ying Zeng, Lei He, Chao Zheng, Zhixue Zhang, Ming Li, Zhengliang Liu, Haixing Dai, Zihao Wu, Lu Zhang, Shu Zhang, Xiaoyan Cai, Xintao Hu, Shijie Zhao, Xi Jiang, Xin Zhang, Xiang Li, Dajiang Zhu, Lei Guo, Dinggang Shen, Junwei Han, Tianming Liu, Jun Liu, and Tuo Zhang. Chatradio-valuer: A chat large language model for generalizable radiology report generation based on multi-institution and multi-system data, 2023.
- [124] Tongxue Zhou, Su Ruan, and Stéphane Canu. A review: Deep learning for medical image segmentation using multi-modality fusion. *Array*, 3:100004, 2019.
- [125] Deyao Zhu, Jun Chen, Xiaonan Shen, Xiang Li, and Mohamed Elhoseiny. Minigtpt-4: Enhancing vision-language understanding with advanced large language models. In *arXiv preprint arXiv:2304.10592*, 2023.
-

A Appendix

A.1 Chest Radiography

Prompt	Image
Assuming you are a radiologist, please conduct a professional evaluation based on the content shown in the following figure. Please describe what you see in the following picture? Judge whether the patient has pneumonia according to the figure below, and point out whether it is COVID-19. Please do not speak humbly, request short and professional answers, and behave like a real doctor.	
Reference answer	Normal
Gemini-1.0-Pro-Vision	The X-ray image shows bilateral interstitial pneumonia. There is no consolidation, so it is not pneumonia. It is most likely COVID-19.
Gemini-1.5-Pro	This is a frontal chest radiograph. The lungs are clear. There is no evidence of pneumonia. A diagnosis of COVID-19 cannot be made from a chest x-ray.
Gemini-1.5-Flash	This is a chest x-ray. The image shows clear lung fields bilaterally. There are no signs of pneumonia or COVID-19.
GPT-4-Turbo	Based on the chest X-ray provided, here is a professional radiological assessment: **Observations** :1. **Lung Fields** : The lung fields appear clear with no evidence of consolidation, significant infiltrates, or areas of increased opacity.2. **Heart Size and Mediastinum** : The heart size is within normal limits, and the mediastinal contours are normal.3. **Diaphragm and Pleural Spaces** : The diaphragm shows normal curvature, and both costophrenic angles are sharp, indicating no pleural effusions.4. **Bony Structures and Soft Tissues** : There are no visible abnormalities in the bones of the thoracic cage or the soft tissues around the lungs. **Assessment** :- The chest X-ray does not show any acute abnormal findings. There are no radiographic signs of pneumonia. The lung fields are clear, and there are no features suggestive of an infectious process. **Diagnosis** :- There is no evidence of pneumonia on this chest X-ray, including no findings suggestive of COVID-19 pneumonia, which often presents with bilateral peripheral ground-glass opacities. **Recommendations** :- If the patient is symptomatic, further evaluation may still be warranted depending on clinical signs and symptoms, but based on this X-ray alone, there is no radiographic evidence of pneumonia.- Continue to monitor and evaluate clinically if symptoms exist, considering other diagnostic methods or tests if necessary.This assessment concludes that the X-ray does not indicate pneumonia or COVID-19 , and the overall appearance suggests a normal chest radiograph.
Claude-3-Opus	Based on the chest X-ray image provided, there are bilateral patchy opacities and areas of consolidation present in both lungs, more prominent in the lower lung zones. The heart size appears normal. No pleural effusions or pneumothorax are evident.Given the bilateral, multifocal nature of the opacities, the imaging findings are highly suspicious for multifocal pneumonia. In the current context of the COVID-19 pandemic, these findings could certainly be consistent with COVID-19 pneumonia. However, it is important to correlate these findings with the patient's clinical presentation, exposure history, and laboratory testing, including COVID-19 PCR, to confirm the diagnosis.Differential diagnoses to consider include other viral pneumonias, atypical bacterial pneumonias, and less likely, non-infectious etiologies such as pulmonary edema or hemorrhage. Follow-up imaging and clinical correlation are recommended to assess for progression or improvement of the findings.In summary, the chest X-ray demonstrates bilateral multifocal opacities suspicious for multifocal pneumonia, which could be consistent with COVID-19 in the appropriate clinical context. Confirmation with laboratory testing and clinical correlation is advised.
GPT-4o	Based on the chest X-ray provided:- **Findings** :- The lung fields are clear with no visible opacities or consolidations.- The heart size appears within normal limits.- The diaphragm and costophrenic angles are sharp.- There are no signs of pleural effusion or pneumothorax.- **Assessment** :- The X-ray does not show any signs of pneumonia.- There are no radiographic indications of COVID-19.The patient's chest X-ray appears normal with no evidence of pneumonia or COVID-19-related changes.

Figure 8: **Chest: Case 2.** In the context of the three-class classification tasks for pneumonia (normal, pneumonia, COVID-19), the green annotation indicates the correctly identified segments, while the red annotation denotes the incorrectly identified segments.

Prompt

Assuming you are a radiologist, please conduct a professional evaluation based on the content shown in the following figure. Please describe what you see in the following picture? Determine whether the patient has pneumonia based on the following diagram? Please do not speak humbly, request short and professional answers, and behave like a real doctor.

Image



Reference answer Pneumonia

Gemini-1.0-Pro-Vision

The X-ray image shows signs of pneumonia. There is consolidation of the lung tissue in the right lower lobe, which is a common finding in pneumonia. The consolidation is caused by the inflammation and fluid that has built up in the lung tissue. There is also a loss of the normal lung markings in the affected area, which is another sign of pneumonia. Based on the X-ray image, it is likely that the patient has pneumonia.

Gemini-1.5-Pro

This is a frontal chest radiograph. The lungs are clear. **There is no evidence of pneumonia.**

Gemini-1.5-Flash

This is a chest x-ray. The image shows bilateral infiltrates **consistent with pneumonia**. It is impossible to determine whether the patient has COVID-19 based on this image alone. Further testing and clinical assessment are needed to confirm the diagnosis.

GPT-4-Turbo

Based on the chest X-ray provided, here is a professional radiological assessment:**Observations**:1. **Lung Fields**: There are patchy areas of increased opacity in both lung fields, which are more pronounced on the right side. These areas may indicate consolidation.2. **Heart Size and Mediastinum**: The cardiac silhouette is obscured partially by the opacities but does not appear enlarged. The mediastinum alignment is normal.3. **Diaphragm and Pleural Spaces**: The diaphragm is visible, but the right costophrenic angle is obscured by opacities, suggesting possible effusion or consolidation extending into the pleural space.4. **Bony Structures and Soft Tissues**: No visible abnormalities in the visible bones of the thoracic cage.**Assessment**: The pattern of patchy opacities, particularly on the right, is suggestive of an infectious process in the lungs, potentially pneumonia.**Diagnosis**: The findings are consistent with pneumonia, given the presence of consolidation. The asymmetrical nature and the volume of opacities could be indicative of bacterial pneumonia; however, the exact etiology cannot be determined solely by X-ray.**Recommendations**: Clinical correlation with the patient's symptoms (such as fever, cough, and dyspnea) is essential to further support the diagnosis. Laboratory tests, including a complete blood count and cultures, should be considered to identify the causative organism. Depending on the patient's clinical status, additional imaging such as CT chest could provide further details if complicated pneumonia is suspected. This X-ray **suggests pneumonia**, and appropriate clinical management should be initiated based on the overall clinical evaluation.

Claude-3-Opus

Based on the chest radiograph provided, there are bilateral patchy opacities present throughout both lung fields, more prominent in the right lung. The opacities appear to be airspace opacities, which are **consistent with multifocal pneumonia**. Given the bilateral distribution and the extent of the opacities, the radiographic findings are highly suggestive of pneumonia. However, clinical correlation with the patient's symptoms, physical examination, and laboratory findings would be necessary for a definitive diagnosis. In summary, the chest radiograph shows bilateral patchy airspace opacities, which are consistent with multifocal pneumonia. Clinical correlation is recommended for a final diagnosis.

GPT-4o

Based on the chest X-ray provided:- **Findings**: The image shows increased opacities in the right middle and lower lung zones. The left lung appears clearer, though there might be some mild increased markings in the lower zones. The heart size is within normal limits. No visible pleural effusion or pneumothorax. **Assessment**: The radiographic findings are suggestive of **right-sided pneumonia**, given the increased opacities and possible consolidation in the right lung. The pattern is more indicative of bacterial pneumonia rather than COVID-19, but clinical correlation and further testing are necessary for a definitive diagnosis. The patient likely has pneumonia, with a bacterial etiology being more probable based on the provided image. Further clinical evaluation and laboratory testing are recommended to confirm the diagnosis and determine the specific cause.

Figure 9: **Chest: Case 3**. In the context of the binary classification task for pneumonia (normal, pneumonia), green annotations indicate correctly recognized fragments, whereas red annotations indicate incorrectly recognized fragments.

Prompt

Assuming you are a radiologist, please conduct a professional evaluation based on the content shown in the following figure. Please describe what you see in the following picture? Determine whether the patient has pneumonia based on the following diagram? Please do not speak humbly, request short and professional answers, and behave like a real doctor.

Image



Reference answer No pneumonia

Gemini-1.0-Pro-Vision

The X-ray shows bilateral infiltrates in the lungs, which is a sign of pneumonia. **The patient has pneumonia.**

Gemini-1.5-Pro

This is a frontal chest radiograph. There are patchy opacities in both lungs **consistent with pneumonia.**

Gemini-1.5-Flash

This is a chest x-ray. The image shows bilateral infiltrates **consistent with pneumonia.** It is impossible to determine whether the patient has COVID-19 based on this image alone. Further testing and clinical assessment are needed to confirm the diagnosis.

GPT-4-Turbo

Based on the chest X-ray provided, here is a professional radiological assessment:**Observations**:1. **Lung Fields**: The lung fields show patchy areas of increased opacity on both sides, with the right side appearing more affected. These areas are suggestive of consolidation.2. **Heart Size and Mediastinum**: The cardiac silhouette appears within normal limits, and there is no evidence of mediastinal shift or enlargement.3. **Diaphragm and Pleural Spaces**: The diaphragm is clearly visible, and no pleural effusions are apparent. The costophrenic angles are sharp.4. **Bony Structures and Soft Tissues**: There are no visible abnormalities in the bones of the thoracic cage or surrounding soft tissues.**Assessment**:- The radiographic appearance suggests an infectious process in the lungs, likely pneumonia, given the presence of bilateral patchy opacities which could represent areas of lung consolidation.**Diagnosis**:- The findings are consistent with pneumonia. The bilateral involvement and patchy nature of the opacities are typical of bacterial or atypical pneumonia, but a specific pathogen cannot be identified based solely on imaging.**Recommendations**:- Clinical correlation with symptoms such as fever, cough, and dyspnea is crucial.- Laboratory investigations, including sputum cultures and blood tests, are recommended to identify the causative organism.- Consider follow-up imaging or a CT scan if there is concern for complications or if the patient does not respond to initial treatment as expected.
This chest X-ray suggests a significant infectious process, **likely pneumonia**, and appropriate clinical management should be pursued based on these findings combined with clinical evaluation.

Claude-3-Opus

Based on the chest X-ray provided, the right lung demonstrates increased opacity and consolidation, particularly in the lower lobe, consistent with a diagnosis of right lower lobe pneumonia.
The left lung appears relatively clear without obvious infiltrates or consolidations.
In summary, this patient's imaging findings are highly suggestive of **right lower lobe pneumonia**. Clinical correlation with the patient's symptoms, physical exam, and laboratory results would provide further confirmation of the diagnosis. Appropriate antibiotic therapy should be initiated promptly.

GPT-4o

Based on the chest X-ray provided:- **Findings**:- There are increased opacities in the right middle and lower lung fields, suggesting possible consolidation.- The left lung appears relatively clear.- The heart size is within normal limits.- No visible pleural effusion or pneumothorax.- **Assessment**:- The radiographic findings are indicative of right-sided pneumonia, with possible consolidation in the right lung.- The etiology of pneumonia cannot be determined solely from the X-ray. Clinical correlation and additional tests (such as bacterial cultures or viral PCR) are necessary to identify the specific cause.The patient **likely has pneumonia**, with significant findings in the right lung. Further clinical evaluation and laboratory tests are recommended to confirm the diagnosis and determine the specific cause.

Figure 10: **Chest: Case 4.** In the context of the binary classification task for pneumonia (normal, pneumonia), green annotations indicate correctly recognized fragments, whereas red annotations indicate incorrectly recognized fragments.

A.2 Ophthalmological Imaging

Prompt	Image
Assuming you are an ophthalmologist, please conduct a professional evaluation based on the content shown in the following figure. Please determine whether the patient has glaucoma based on fundus figure? Please estimate the coordinate position of the macular fovea, starting from the top left corner of the image as the (0,0) coordinate, increasing to the right along the x-axis and decreasing along the y-axis. Please do not speak humbly, ask for short and professional answers, and act like a real doctor.	
Reference answer	Glaucoma Fovea: (1402.13, 1064.83)
Gemini-1.0-Pro-Vision	
Based on the fundus image, the patient does not have glaucoma . The optic disc is normal in size and shape, and there is no evidence of optic nerve damage. The macular fovea is located at (250, 250) .	
Gemini-1.5-Pro	
No evidence of glaucoma . Optic nerve appears normal. Macula approximately located at (600, -200) .	
Gemini-1.5-Flash	
No glaucoma . Optic nerve head appears normal. Macular fovea approximately (400, -200) .	
GPT-4-Turbo	
Based on the fundus photograph provided: Findings: Optic Disc: The optic disc, highlighted within the circle, appears healthy with a normal cup-to-disc ratio. There is no visible excessive cupping or pallor that would typically indicate glaucoma. Blood Vessels: The blood vessels emanating from the optic disc show normal branching and caliber, without signs of bending, nicking, or copper wiring. Retinal Features: The retina around the optic disc and extending towards the macula shows no signs of swelling, hemorrhages, or exudates. Glaucoma Assessment: There are no apparent signs of glaucoma in this image such as significant optic disc cupping or nerve fiber layer damage. To definitively rule out glaucoma, further examinations including intraocular pressure measurement, visual field testing, and optical coherence tomography (OCT) are necessary. Estimation of Macular Fovea Coordinates: Position: The macular fovea is typically situated horizontally in line with the optic disc but slightly lower. It is usually located approximately 2 disc diameters lateral (to the right) from the center of the optic disc. Estimated Coordinates: Based on the structure of the fundus: X-coordinate: Roughly 70-75% of the way from the left edge of the image. Y-coordinate: Approximately 50-55% of the way from the top edge of the image, given that the macula is slightly lower than the mid-horizontal axis of the optic disc. Recommendations: Comprehensive Eye Exam: Including intraocular pressure (IOP) measurements and visual field analysis to fully assess the risk or presence of glaucoma. Regular Monitoring: Scheduled follow-ups for early detection of any changes that might indicate the development of glaucoma or other retinal conditions. Conclusion: From the visible details in this image, there are no evident signs of glaucoma. The estimated location of the macular fovea suggests it is within the normal range relative to the optic disc. Comprehensive testing is recommended for a conclusive evaluation.	
Claude-3-Opus	
Based on the provided fundus photograph, there are no clear signs of glaucomatous optic neuropathy . The optic nerve head appears healthy with a normal cup-to-disc ratio and no obvious notching or thinning of the neuroretinal rim. However, a single fundus photo is not sufficient to definitively rule out glaucoma. Further testing such as optical coherence tomography (OCT), visual field testing, and intraocular pressure measurement would provide a more comprehensive assessment. The image shows a normal fundus with visible retinal blood vessels radiating from the optic disc. The macula, located temporal to the optic disc, appears healthy with a normal foveal light reflex. Assuming the top left corner of the image represents coordinate (0,0), I estimate the center of the macular fovea is located at approximately (475, 280) based on the provided resolution. In summary, while no overt signs of glaucoma are apparent, additional diagnostic testing is recommended to fully evaluate the patient's glaucoma status. The macula and fovea appear normal in this fundus photograph.	
GPT-4o	
### Evaluation of Fundus Image Glaucoma Assessment: In this fundus image, the optic disc shows a large cup-to-disc ratio with evident cupping. The thinning of the neuroretinal rim suggests glaucomatous optic neuropathy . These findings are consistent with glaucoma. For confirmation, additional tests such as intraocular pressure measurement, visual field analysis, and optical coherence tomography (OCT) should be performed. Macular Fovea Position: The macular fovea, indicated by the purple cross, is approximately located at coordinates (1150, 950) in the image, assuming the top left corner is (0,0). Further clinical examination and diagnostic tests are recommended to confirm the diagnosis of glaucoma.	

Figure 11: **Ophthalmological Imaging: Case 2.** Diagnosis of glaucoma and the task of localizing the macular fovea, the green annotation indicates the correctly identified segments, while the red annotation denotes the incorrectly identified segments.

Prompt

Assuming you are an ophthalmologist, please conduct a professional evaluation based on the content shown in the following figure. Please determine whether the patient has glaucoma based on fundus figure? Please estimate the coordinate position of the macular fovea, starting from the top left corner of the image as the (0,0) coordinate, increasing to the right along the x-axis and decreasing along the y-axis. Please do not speak humbly, ask for short and professional answers, and act like a real doctor.

Image



Reference answer **No glaucoma Fovea: (1047.12, 1057.25)**

Gemini-1.0-Pro-Vision

The optic disc is slightly enlarged, and the optic cup is deep and wide. The retinal nerve fiber layer is thinned. **These are all signs of glaucoma. The macular fovea is located at (220, -220).**

Gemini-1.5-Pro

Glaucoma. Optic nerve head cupping present. **Macular fovea approximately (400, -200).**

Gemini-1.5-Flash

The patient has glaucoma. The optic nerve head shows cupping with rim thinning. **The macular fovea is located at approximately (400, -200).**

GPT-4-Turbo

Based on the fundus photograph provided:

Findings:

- **Optic Disc:** The optic disc appears within the circled area, showing no evident cupping or pallor. The cup-to-disc ratio looks normal, and there is no visible sign of nerve fiber layer thinning.
- **Blood Vessels:** Retinal blood vessels appear healthy without signs of excessive bending or narrowing that might suggest high intraocular pressure.
- **Retinal Condition:** The retina around the optic disc and macula shows no signs of hemorrhages, exudates, or significant abnormalities.

Glaucoma Assessment:

- **There are no typical signs of glaucoma such as optic disc cupping**, notching, or nerve fiber layer defects visible in this image. However, confirming the absence of glaucoma requires comprehensive examination including intraocular pressure measurement, visual field tests, and possibly an optical coherence tomography (OCT) scan.

Estimation of Macular Fovea Coordinates:

- Based on the orientation and anatomy typical of fundus images, and considering the top left corner of the image as the (0,0) coordinate:
- **X-coordinate:** The macular fovea typically lies directly horizontal to the optic disc, about 2 disc diameters away. Assuming the disc is roughly at 1/3 from the left edge, the macula would be near the center of the image. Estimating the macula's X-coordinate would be approximately at 65-75% of the image's width.
- **Y-coordinate:** The macula is slightly below the horizontal midline of the optic disc, approximately at 40-50% down from the top of the image.

Recommendations:

- **Confirmatory Testing:** Although no evident signs of glaucoma are visible, additional diagnostic tests such as intraocular pressure measurement, gonioscopy, and visual field analysis are necessary for a complete evaluation.
- **Regular Monitoring:** Even if glaucoma is ruled out, regular eye exams are recommended to monitor changes, especially in patients at higher risk for eye diseases.

Conclusion:

This fundus photograph does not show overt signs of glaucoma. **The macular fovea appears to be positioned around the center and slightly below the midline of the image, indicative of normal positioning relative to the optic disc.** Further tests are advised to ensure comprehensive evaluation.

Figure 12: **Ophthalmological Imaging: Case 3(Part 1)**. Diagnosis of glaucoma and the task of localizing the macular fovea, the green annotation indicates the correctly identified segments, while the red annotation denotes the incorrectly identified segments.

Prompt

Assuming you are an ophthalmologist, please conduct a professional evaluation based on the content shown in the following figure. Please determine whether the patient has glaucoma based on fundus figure? Please estimate the coordinate position of the macular fovea, starting from the top left corner of the image as the (0,0) coordinate, increasing to the right along the x-axis and decreasing along the y-axis. Please do not speak humbly, ask for short and professional answers, and act like a real doctor.

Image



Reference answer **No glaucoma Fovea: (1047.12, 1057.25)**

Claude-3-Opus

Based on the fundus image provided, there are a few key observations:

1. The optic disc appears enlarged with increased cupping, which is suspicious for glaucomatous changes. The cup-to-disc ratio appears to be approximately 0.7-0.8.
2. There is no obvious notching or focal thinning of the neuroretinal rim. However, the inferior rim in particular looks quite thin.
3. The retinal nerve fiber layer also shows some signs of thinning, especially inferiorly.
4. Retinal vessels and macula appear normal, with no signs of diabetic retinopathy or macular degeneration.
5. Estimating the coordinate position of the fovea, with the top left corner as (0,0) and assuming an image resolution of approximately 800x800 pixels, the fovea appears to **be centered around the coordinate (475, 380)**.

In summary, while a conclusive diagnosis of glaucoma cannot be made based on a single fundus photo alone, the enlarged cup-to-disc ratio and neuroretinal rim thinning are **highly suspicious for glaucoma**. I would recommend further diagnostic testing including optical coherence tomography (OCT), visual field testing, and intraocular pressure measurement to confirm the diagnosis and stage the severity of any glaucomatous damage. Close monitoring and potential treatment initiation would then be warranted based on those results.

GPT-4o

Evaluation of Fundus Image

Glaucoma Assessment:

In this fundus image, the optic disc shows a significant cup-to-disc ratio, with notable cupping. **This suggests glaucomatous optic neuropathy.** The thinning of the neuroretinal rim and the pallor of the optic disc further support the suspicion of glaucoma. Confirmatory tests such as intraocular pressure measurement, visual field analysis, and optical coherence tomography (OCT) are recommended for a definitive diagnosis.

Macular Fovea Position:

The macular fovea, indicated by the purple cross, is **approximately located at coordinates (1100, 1100)** in the image, assuming the top left corner is (0,0). Further clinical examination and diagnostic tests are recommended to confirm the diagnosis of glaucoma.

Figure 13: **Ophthalmological Imaging: Case 3(Part 2)**. Diagnosis of glaucoma and the task of localizing the macular fovea, the green annotation indicates the correctly identified segments, while the red annotation denotes the incorrectly identified segments.

A.3 Endoscopic Imaging

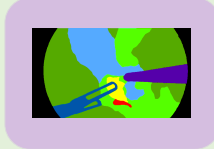
Prompt	Image	Reference answer
<p>Assuming you are a surgical expert, please provide a detailed description of the content shown in the following figure. What did you see? Please do not speak humbly and act like a real doctor.</p>		
Gemini-1.0-Pro-Vision <p>The image shows a laparoscopic view of the stomach. The stomach is the J-shaped organ that sits in the upper left quadrant of the abdomen. It is responsible for the digestion of food. The image shows the stomach with a small incision in it. This incision is made in order to perform a gastrectomy, which is a surgical procedure to remove part of the stomach. The surgeon is using a laparoscope, which is a small camera inserted into the abdomen, to view the stomach and perform the surgery.</p>		
Gemini-1.5-Pro <p>This is a laparoscopic image. The gallbladder is inflamed and being grasped by laparoscopic instruments. There is evidence of purulent material consistent with acute cholecystitis.</p>		
Gemini-1.5-Flash <p>This is a laparoscopic view of the abdomen. The image shows the liver, the gallbladder, and a portion of the small intestine. The gallbladder appears to be distended and inflamed. There are surgical instruments present in the field, likely for a laparoscopic cholecystectomy to remove the gallbladder. The patient is likely experiencing symptoms of cholecystitis, such as abdominal pain, nausea, and vomiting.</p>		
GPT-4-Turbo <p>The image depicts a laparoscopic surgical procedure being performed in the abdominal cavity. Here's a detailed description based on the visual cues:</p> <ol style="list-style-type: none">Procedure Context: The image shows a laparoscopic forceps handling what appears to be a small, nodular lesion or mass in the omentum, which is a layer of fatty tissue that drapes over the abdominal organs. The forceps are likely being used for either biopsy or excision of this mass.Surgical Environment: The surrounding anatomy includes the liver (upper left part of the image), which looks normal in texture and color, suggesting that the focus of this procedure is not related to the liver but likely the omentum or nearby structures.Lesion Appearance: The lesion appears relatively small, with a pinkish hue, slightly different in color from the surrounding fatty tissue, suggesting it could be a benign lesion like an omental cyst or lipoma, or potentially a metastatic deposit if there's an existing diagnosis of cancer.Surgical Technique: The laparoscopic approach shown uses minimally invasive techniques, which generally allow for quicker recovery, reduced pain, and less scarring compared to open surgery. The presence of a laparoscopic clip applier (the tool in the image) indicates that the surgeon might be about to secure or cut a blood vessel or tissue structure, likely related to the removal or biopsy of the lesion. <p>Given the context and tools visible, this procedure seems to be focused on either diagnostic evaluation or treatment of a localized issue within the omentum or adjacent tissues. Further histopathological examination of the lesion will be necessary to determine its nature and guide further treatment.</p>		

Figure 15: **Endoscopic: Case 2(Part 1)**. The task of abdominal segmentation during the surgical process employs green markings to denote correct answers, red markings to indicate incorrect answers, and yellow markings to highlight noteworthy content.



Figure 16: **Endoscopic: Case 2(Part 2)**. The task of abdominal segmentation during the surgical process employs green markings to denote correct answers, red markings to indicate incorrect answers, and yellow markings to highlight noteworthy content.



Figure 17: **Endoscopic: Case 3(Part 1)**. The segmentation task during cholecystectomy surgery uses green markings to indicate correct answers, red markings to indicate incorrect answers, and yellow markings to highlight noteworthy content.

Prompt	Image	Reference answer
<p>Assuming you are a surgical expert, please provide a detailed description of the content shown in the following figure. What did you see? Please do not speak humbly and act like a real doctor.</p>		
<p>Claude-3-Opus</p>		
<p>Based on the image, we are looking at an endoscopic view of the gastrointestinal tract, most likely the colon or large intestine. The image shows the mucosa and lumen of the colon through a colonoscope. The mucosa appears highly abnormal with an irregular, nodular and ulcerated appearance. There are areas of necrosis, inflammation and possible bleeding or exudate. The lumen is narrowed, suggesting stricturing or obstruction of the bowel.</p> <p>Given the appearance, the most likely diagnosis is a malignant neoplasm of the colon, such as a colorectal adenocarcinoma in an advanced stage. The lesion appears to be circumferential, involving a significant portion of the colonic wall. Biopsies would need to be taken to confirm the diagnosis histologically.</p> <p>Alternate differential diagnoses could include severe inflammatory conditions like Crohn's disease or ulcerative colitis, or more rare neoplasms like lymphoma or gastrointestinal stromal tumor. However, the appearance is highly suggestive of an advanced colorectal adenocarcinoma.</p> <p>Staging with CT scans would be required to assess for local invasion and distant metastases. Treatment would likely involve surgical resection if feasible, along with chemotherapy and possibly radiation depending on the stage and operability. The prognosis will depend on the final staging, but given the advanced endoscopic appearance, survival rates would likely be quite low.</p> <p>In summary, this is a concerning endoscopic finding that requires immediate action and a multidisciplinary approach to properly diagnose and treat this probable colorectal malignancy. Prompt biopsies and staging are the next crucial steps in management.</p>		
<p>GPT-4o</p>		
<p>The image shows a laparoscopic view of the abdominal cavity, focusing on the hepatic region and surrounding structures during a surgical procedure.</p> <p>**Description:**</p> <ol style="list-style-type: none"> **Tissues and Structures:** <ul style="list-style-type: none"> - **Liver:** The reddish-brown organ dominates the image, indicating that the view is within the upper right quadrant of the abdomen. - **Fibrous Tissue and Fat:** There is visible fibrous and fatty tissue (yellowish and white) in the upper part of the image, likely representing the peritoneum and surrounding connective tissue. - **Blood Vessels:** Several small blood vessels are visible, with minor bleeding present, indicating active dissection. **Surgical Instruments:** <ul style="list-style-type: none"> - **Electrocautery Device:** A surgical tool, likely an electrocautery probe, is being used to dissect or coagulate tissues, as evidenced by its pointed tip and the surrounding tissue reaction. <p>**Surgical Context:**</p> <p>The procedure seems to involve the dissection or resection of tissues near the liver, possibly related to the gallbladder (cholecystectomy) or addressing a hepatic lesion or abscess.</p> <p>**Findings:**</p> <ul style="list-style-type: none"> - **Dissection Site:** The presence of fibrous tissue, minor bleeding, and active use of an electrocautery device suggests ongoing dissection, possibly separating the gallbladder from the liver bed or addressing adhesions. - **Minor Bleeding:** The image shows some minor bleeding, which is being controlled using the electrocautery device. <p>**Recommendations:**</p> <ul style="list-style-type: none"> - **Hemostasis:** Continue careful hemostasis to control bleeding. - **Tissue Handling:** Maintain gentle tissue handling to minimize further damage and ensure clear visualization of anatomical structures. - **Pathology Examination:** If tissue removal is involved, ensure that samples are sent for pathological analysis. <p>**Conclusion:**</p> <p>The image depicts a laparoscopic procedure in the hepatic region with active dissection using an electrocautery device. The exact nature of the surgery is not fully clear, but it likely involves the gallbladder or nearby hepatic structures. Careful surgical technique and hemostasis are essential to ensure a successful outcome.</p>		

Figure 18: **Endoscopic: Case 3(Part 2)**. The segmentation task during cholecystectomy surgery uses green markings to indicate correct answers, red markings to indicate incorrect answers, and yellow markings to highlight noteworthy content.



Figure 19: **Endoscopic: Case 4(Part 1)**. The task of colon polyp localization and segmentation uses green markings to represent correct answers, red markings to represent incorrect answers, and yellow markings to highlight noteworthy content.



Figure 20: **Endoscopic: Case 4(Part 2)**. The task of colon polyp localization and segmentation uses green markings to represent correct answers, red markings to represent incorrect answers, and yellow markings to highlight noteworthy content.

A.4 Dermatological Imaging

Prompt	Image
<p>Assuming you are a dermatologist, please conduct a professional evaluation based on the content shown in the following figure. Is there any lesion in the following picture? If so, please provide a brief description of the lesion and explain what it is. Please do not speak humbly, ask for a brief and professional answer, and act like a real doctor.</p>	
Reference answer	basal cell carcinoma
Gemini-1.0-Pro-Vision	
<p>There is a pigmented lesion on the patient's skin. The lesion is round, with a diameter of about 5 mm. It is light brown in color, with a slightly raised surface. The lesion is surrounded by a thin, white halo.</p> <p>The lesion is most likely a seborrheic keratosis. Seborrheic keratoses are common, benign growths that are found on the skin. They are caused by the overgrowth of keratinocytes, which are the cells that make up the skin's outer layer. Seborrheic keratoses are typically harmless, but they can sometimes be itchy or irritated.</p> <p>Treatment for seborrheic keratoses is not necessary. However, if the lesion is bothersome, it can be removed by a dermatologist. There are a number of different methods that can be used to remove seborrheic keratoses, including surgery, laser therapy, and cryotherapy.</p>	
Gemini-1.5-Pro	
<p>Yes, there is a lesion. This is a blue nevus. It is a benign melanocytic proliferation characterized by a blue-gray to black color.</p>	
Gemini-1.5-Flash	
<p>This is concerning. The lesion in the image, with its irregular borders and multiple colors, has features suggestive of melanoma. It requires immediate referral to a dermatologist for biopsy and further evaluation.</p>	
GPT-4-Turbo	
<p>The image provided appears to be another dermoscopy photo, commonly used in dermatology to examine skin lesions at a high magnification.</p> <p>Observation:- The lesion shows a mix of light brown and dark blue-black pigmentation, with a reddish background. There are visible black dots and globules, which are typical dermoscopic features. The pattern is somewhat irregular, with asymmetric distribution of pigments and structures.</p> <p>Assessment:- This lesion, given the presence of multiple colors (brown, black, and red), black dots, and an irregular pattern, could represent a melanocytic lesion. The characteristics observed, especially the blue-black pigment and irregularity, are concerning features often associated with melanoma.</p> <p>Diagnosis:- The lesion has several suspicious features that could indicate a malignant melanoma, which is a potentially aggressive form of skin cancer. The diagnosis would be provisional based on this dermoscopy image alone and requires further evaluation.</p> <p>Recommendations:- It is strongly recommended to perform an excisional biopsy of the lesion for histopathological examination. This is the best approach to determine if the lesion is benign or malignant. A thorough skin examination should also be conducted to check for any other suspicious lesions.</p> <p>Conclusion:- The features noted on dermoscopy are concerning for melanoma. Immediate dermatological consultation and biopsy are advised to determine the appropriate treatment and ensure timely management if confirmed to be malignant.</p>	
Claude-3-Opus	
<p>Based on the provided image, there appears to be a skin lesion present. The lesion has the following characteristics: Irregular borders- Asymmetric shape- Non-uniform color, with darker and lighter areas- Diameter larger than 6mm Given these features, the lesion is suspicious for melanoma, a potentially serious form of skin cancer. However, to confirm the diagnosis, a biopsy would be necessary for histopathological examination. As a dermatologist, my recommendation would be to perform an excisional biopsy to remove the entire lesion and a margin of normal-appearing skin around it. This will allow for a definitive diagnosis and guide further treatment if needed. It is essential to monitor your skin regularly for any new or changing lesions and to seek prompt medical attention for any suspicious findings. Early detection and treatment of melanoma are critical for the best possible outcome.</p>	
GPT-4o	
<p>Based on the dermoscopic image provided:-</p> <p>Findings:- There is an irregularly shaped lesion with varying pigmentation.- The lesion exhibits a mix of light pink, blue, and brown colors.- Presence of irregular dots and globules within the lesion.-</p> <p>Assessment:- The features observed are concerning for melanoma, particularly due to the irregular shape, mixed colors, and the presence of blue and black structures.- Further evaluation, including a biopsy, is recommended to confirm the diagnosis and rule out malignancy. The lesion presents characteristics suggestive of melanoma, necessitating immediate further investigation.</p>	

Figure 21: **Skin: Case 2.** The nine classification tasks for skin diseases utilize green markings to denote correct answers and red markings to indicate incorrect answers.

Prompt

Image

Assuming you are a dermatologist, please conduct a professional evaluation based on the content shown in the following picture. Is the tumor in the following picture benign or malignant? Please answer benign or malignant and provide your reasons. Please do not speak humbly, request short and professional answers, and behave like a real doctor.



Reference answer

benign

Gemini-1.0-Pro-Vision

The tumor is **benign**.
The tumor is a compound nevus. It is a benign tumor that is made up of both melanocytes and keratinocytes. Melanocytes are the cells that produce melanin, which is the pigment that gives skin its color. Keratinocytes are the cells that make up the outer layer of the skin. Compound nevi are usually round or oval and are brown or black in color. They are often found on the face, neck, and arms. Compound nevi are not cancerous and do not need to be treated.

Gemini-1.5-Pro

Benign. This lesion demonstrates symmetry, a well-defined border, and uniform color, all features of benign lesions.

Gemini-1.5-Flash

Malignant. The lesion has irregular borders and a variety of colors, suggesting melanoma. A biopsy is needed for definitive diagnosis.

GPT-4-Turbo

Based on the dermoscopy image provided, here is a professional evaluation of the lesion:****Observation****:

- The lesion exhibits a dense cluster of dark brown to black pigmentation, which is irregularly shaped and unevenly distributed. The background skin shows a uniform coloration with no visible structures.

****Assessment****:

- The lesion shows characteristics concerning for a melanocytic nevus (mole) or melanoma, particularly due to its irregular shape and uneven color distribution.

****Diagnosis****:

- Given the visual complexity and irregularity, the lesion could potentially be malignant. It exhibits features suggestive of **melanoma, such as asymmetry, border irregularity, multiple colors, and a diameter that appears to be less than 6 mm but irregular.**

****Recommendations****:

- An excisional biopsy is highly recommended for accurate histopathological diagnosis. This will determine whether the lesion is benign (like a dysplastic nevus) or malignant (melanoma).
- Comprehensive skin examination and possibly total body skin photography for monitoring are advised, especially if the biopsy confirms a melanoma.

****Conclusion****:

- The lesion is suspicious for melanoma based on dermoscopy characteristics. Immediate dermatological action in the form of a biopsy is imperative to confirm the diagnosis and guide further treatment.

Claude-3-Opus

Based on the provided image, **I cannot definitively determine if the lesion is benign or malignant.** The image shows a small, dark irregular lesion on the skin, which has some concerning features that could potentially indicate a malignant melanoma, such as asymmetry and color variation. However, additional information and tests would be needed to make a definitive diagnosis, such as the size of the lesion, any recent changes, and the results of a biopsy. My recommendation would be to have this lesion evaluated in-person by a dermatologist as soon as possible for a thorough assessment and potential biopsy, as early detection is crucial if this does turn out to be a melanoma. Let me know if you have any other questions!

GPT-4o

Based on the dermoscopic image provided:- ****Assessment****:- ****Malignant.****- ****Reasons****:- **The lesion is asymmetrical with irregular, uneven borders.- The pigmentation is uneven with multiple shades of brown.**- The overall appearance is suggestive of melanoma due to these atypical features. Immediate further investigation, including a biopsy, is recommended to confirm the diagnosis and plan appropriate treatment.

Figure 22: **Skin: Case 3.** The benign and malignant classification task of skin nevi employs green markers to denote correct answers, red markers to denote incorrect answers, and yellow markers to highlight noteworthy content.

Prompt	Image	Reference answer
<p>Assuming you are a dermatologist, please conduct a professional evaluation based on the content shown in the following picture. What do you see in the following picture? Where is the location of the lesion? Please do not speak humbly, ask for short and professional answers, and act like a real doctor.</p>		
<p>Gemini-1.0-Pro-Vision</p>		
<p>It is a pigmented lesion with asymmetry, an irregular border, variegated color, and diameter greater than 6 mm. It is located on the patient's back. I would recommend a biopsy to rule out melanoma.</p>		
<p>Gemini-1.5-Pro</p>		
<p>Pigmented lesion with irregular borders. Location cannot be determined from image alone.</p>		
<p>Gemini-1.5-Flash</p>		
<p>The picture shows a pigmented lesion on the skin, appearing to be a nevus (mole). The lesion is located on the patient's skin, likely a superficial area. However, a clinical examination and potentially a biopsy are required to confirm the diagnosis and determine its nature.</p>		
<p>GPT-4-Turbo</p>		
<p>The image you've shared shows a close-up view of a skin lesion. It appears to be a nevus, commonly known as a mole, characterized by a dark, centralized color with irregular edges and varying shades of brown and black. The surrounding skin is pink, which might indicate inflammation or irritation. Dermoscopy, a tool commonly used by dermatologists for such evaluations, reveals a reticular pattern, which is typical but warrants careful observation for any signs of dysplasia (abnormal development of cells). I cannot definitively identify the body location of the lesion based on this image alone, as this detail depends on wider context not provided in the close-up view. For a professional diagnosis, a full examination of the lesion in the context of its location on the body, the patient's skin type, personal and family medical history, and potentially a biopsy would be required. Please consult a dermatologist in person for an accurate diagnosis and advice on any necessary treatment.</p>		
<p>Claude-3-Opus</p>		
<p>Based on the provided image, the lesion appears to be a pigmented nevus, commonly known as a mole, located on the skin. The mole has an irregular border and a dark red to purple color. The exact body location is unclear from this close-up view, but it seems to be on a region of fair skin, possibly the trunk or a limb. As a dermatologist, I would recommend monitoring this lesion closely for any changes in size, shape, or color. While the appearance is consistent with a benign nevus, any rapid or concerning changes warrant further evaluation, such as dermoscopy or biopsy, to rule out the possibility of malignancy, such as melanoma. Encouraging the patient to perform regular self-skin exams and to follow up for periodic professional skin checks is advisable.</p>		
<p>GPT-4o</p>		
<p>Based on the dermoscopic image provided:</p> <ul style="list-style-type: none"> - Findings: <ul style="list-style-type: none"> - The image shows a pigmented lesion with irregular borders and varying shades of brown. - The pigmentation is uneven and asymmetrical. - There are some visible hair structures near the lesion. - Assessment: <ul style="list-style-type: none"> - The lesion is suspicious for melanoma due to its asymmetry, irregular borders, and heterogeneous pigmentation. - Location: <ul style="list-style-type: none"> - The exact anatomical location cannot be determined solely from the image. However, it appears to be on skin with visible hair follicles, suggesting a possible location on a hair-bearing area such as the trunk, limbs, or scalp. <p>Further evaluation, including a biopsy, is recommended to confirm the diagnosis and determine the appropriate treatment plan.</p>		

Figure 23: **Skin: Case 4.** The seven classification recognition and detection task of skin diseases utilizes yellow markers to emphasize noteworthy content.

A.5 Dental Imaging

Prompt	Image
<p>Assuming you are a dentist, please conduct a professional assessment based on the content shown in the following figure. Please divide the teeth in the following image into four regions: upper right region, upper left region, lower left region, and lower right region. Please accurately state the number of teeth in each area of the picture, as there may be defects inside. Please do not speak humbly, ask for short and professional answers, and act like a real doctor.</p>	
Reference answer	No reference information
Gemini-1.0-Pro-Vision	
<p>**Upper right region: 7 teeth.**Upper left region: 6 teeth.**Lower left region: 5 teeth.**Lower right region: 6 teeth.**Total: 24 teeth.</p>	
Gemini-1.5-Pro	
<p>Upper Right: 7 teeth Upper Left: 7 teeth Lower Left: 8 teeth Lower Right: 8 teeth</p>	
Gemini-1.5-Flash	
<p>Upper right region: 3 teeth Upper left region: 3 teeth Lower left region: 5 teeth Lower right region: 5 teeth</p>	
GPT-4-Turbo	
<p>Based on the panoramic dental X-ray provided, here is a professional assessment of the dental structures visible:**Upper Right Region (Quadrant 1)**- **Number of Teeth**: 8 teeth are present. This quadrant includes teeth from the second molar to the central incisor, with the third molar (wisdom tooth) not visible, suggesting it may be missing or not developed.**Upper Left Region (Quadrant 2)**- **Number of Teeth**: 8 teeth are present, from the central incisor to the second molar, similar to the upper right quadrant, with the third molar also not visible.**Lower Left Region (Quadrant 3)**- **Number of Teeth**: 6 teeth are visible. Notably, several teeth including the third molar are missing, and there appears to be some bone loss indicating possible previous extractions or periodontal issues.**Lower Right Region (Quadrant 4)**- **Number of Teeth**: 5 teeth are present. This quadrant shows significant tooth loss and similar bone degradation as seen in the lower left quadrant, with the third molar and several other teeth absent.**Overall Assessment**:- There is significant tooth loss particularly in the lower quadrants, which might be associated with previous extractions or periodontal disease. The upper quadrants are more intact but also missing the third molars. Further clinical evaluation and possibly additional imaging (like periapical X-rays) would be necessary to assess periodontal health, check for root integrity, and plan any potential restorative treatments.This assessment, based on the X-ray provided, suggests a need for comprehensive dental evaluation and possibly interventions to manage the significant dental issues noted in the lower quadrants.</p>	
Claude-3-Opus	
<p>Based on the dental X-ray provided, here is my professional assessment of the number of teeth present in each region: Upper right region: 8 teeth visible Upper left region: 8 teeth visible Lower left region: 7 teeth visible Lower right region: 7 teeth visible In total, 30 teeth are visible in this panoramic radiograph. The lower left and right regions each appear to be missing 1 tooth, likely the third molars (wisdom teeth). No obvious defects or pathologies are noted in the visible teeth, but a full oral examination and additional imaging would be required to comprehensively evaluate dental health.</p>	
GPT-4o	
<p>### Dental Panoramic X-ray Assessment**Upper Right Region**:- Number of teeth: 3- Observation: There are three teeth visible, with no third molar (wisdom tooth) present. Some teeth may be missing.**Upper Left Region**:- Number of teeth: 3- Observation: Three teeth are visible, including some with crowns. The third molar (wisdom tooth) is absent, and there are missing teeth.**Lower Left Region**:- Number of teeth: 8- Observation: All eight teeth are visible, including molars, premolars, and anterior teeth. The third molar appears to be missing.**Lower Right Region**:- Number of teeth: 8- Observation: Eight teeth are visible, including molars, premolars, and anterior teeth. The third molar appears to be missing.**Summary**:The total number of teeth present is 22. There are several missing teeth, particularly in the upper regions. Further evaluation, including a clinical examination, is recommended to assess the condition of existing teeth and any potential need for prosthetics or further treatment.</p>	

Figure 24: **Dental Image: Case 2.** The task involves quantifying the number of teeth and identifying anomalies in dental X-rays, with critical information highlighted in yellow.

Prompt

Assuming you are a dentist, please conduct a professional assessment based on the content shown in the following figure. Please divide the teeth in the following image into four regions: upper right region, upper left region, lower left region, and lower right region. Please accurately state the number of teeth in each area of the picture, as there may be defects inside. Please do not speak humbly, ask for short and professional answers, and act like a real doctor.

Image



Reference answer

No reference information

Gemini-1.0-Pro-Vision

****Upper right region:** 8 teeth**Upper left region:** 7 teeth**Lower left region:** 8 teeth**Lower right region:** 8 teeth**Total:** 31 teeth There are 31 teeth in total, with 8 in the upper right region, 7 in the upper left region, 8 in the lower left region, and 8 in the lower right region. **There are no obvious defects in the teeth.****

Gemini-1.5-Pro

Upper right: 8 teeth Upper left: 8 teeth Lower left: 8 teeth Lower right: 8 teeth

Gemini-1.5-Flash

Upper right region: 5 teeth Upper left region: 5 teeth Lower left region: 6 teeth Lower right region: 6 teeth

GPT-4-Turbo

Based on the panoramic dental X-ray provided, here is a professional assessment of the dental structures visible:****Upper Right Region (Quadrant 1)**- **Number of Teeth:** 7 teeth are visible, including the second molar. **The third molar (wisdom tooth) is missing, and there appears to be a crown on one of the molars.****Upper Left Region (Quadrant 2)**- **Number of Teeth:** 8 teeth are present, all the way from the third molar (wisdom tooth) to the central incisor. **This quadrant appears to have a full complement of teeth, including restorations visible on the premolars.****Lower Left Region (Quadrant 3)**- **Number of Teeth:** 8 teeth are visible. **This quadrant includes all teeth from the third molar to the central incisor, indicating no missing teeth and showing a dental restoration on one of the molars.****Lower Right Region (Quadrant 4)**- **Number of Teeth:** 7 teeth are present. **The third molar is absent, and there is a dental restoration visible on the first molar.****Overall Assessment**:- **This dental X-ray shows a full complement of teeth in the upper left and lower left regions, with absent third molars in the upper right and lower right regions. There are several restorations in place, suggesting previous dental treatments. The alignment of teeth appears normal without significant crowding or spacing issues.** However, the presence of restorative work warrants regular dental check-ups to monitor the integrity of these restorations and the overall dental health.Further clinical evaluation would be necessary to assess the health of the gums, check for any signs of decay not visible on the X-ray, and possibly update any needed dental work.**

Claude-3-Opus

Based on my analysis of the dental X-ray provided, here are my findings:
 Upper right region: 8 teeth present. **The wisdom tooth (#1) appears to be impacted.**
 Upper left region: 8 teeth present. **No apparent abnormalities.**
 Lower left region: 7 teeth present. **The wisdom tooth (#17) appears to be missing.**
 Lower right region: 8 teeth present, **including the wisdom tooth (#32).**
 In total, **there are 31 teeth visible in the panoramic radiograph. The missing tooth is likely the lower left wisdom tooth (#17). The upper right wisdom tooth (#1) is impacted and may require further evaluation and possibly extraction.**No other significant dental pathologies or abnormalities are immediately evident based on this single X-ray. A comprehensive clinical examination and additional radiographs would be necessary for a complete diagnostic assessment.

GPT-4o

Based on the panoramic dental X-ray provided:
****Upper Right Region:**- Contains 8 teeth, including third molar (wisdom tooth).
 Upper Left Region:- Contains 8 teeth, including third molar (wisdom tooth).
 Lower Left Region:- Contains 7 teeth, with one missing third molar.
 Lower Right Region:- Contains 8 teeth, including third molar (wisdom tooth).
There is evidence of dental restorations (fillings) in the upper regions. No significant pathology noted in the provided image.**

Figure 25: **Dental Image: Case 3.** The task involves quantifying the number of teeth and identifying anomalies in dental X-rays, with critical information highlighted in yellow.

Prompt

Assuming you are a dentist, please conduct a professional assessment based on the content shown in the following figure. Please divide the teeth in the following image into four regions: upper right region, upper left region, lower left region, and lower right region. Please accurately state the number of teeth in each area of the picture, as there may be defects inside. Please do not speak humbly, ask for short and professional answers, and act like a real doctor.

Image



Reference answer

No reference information

Gemini-1.0-Pro-Vision

****Upper right region:** 8 teeth**Upper left region:** 7 teeth**Lower left region:** 8 teeth**Lower right region:** 8 teeth**Total:** 31 teeth**

Gemini-1.5-Pro

Upper Right: 8 teeth Upper Left: 7 teeth Lower Left: 8 teeth Lower Right: 8 teeth

Gemini-1.5-Flash

Upper right region: 4 teeth Upper left region: 4 teeth Lower left region: 4 teeth Lower right region: 5 teeth

GPT-4-Turbo

Based on the panoramic dental X-ray provided, here is a professional assessment of the dental structures visible:****Upper Right Region (Quadrant 1)**- **Number of Teeth:** 3 teeth are visible. This quadrant shows significant tooth loss with only a few posterior teeth remaining. There are multiple dental restorations and possibly a bridge visible.**Upper Left Region (Quadrant 2)**- **Number of Teeth:** 4 teeth are visible, with restorative work on several of these. This quadrant similarly shows extensive tooth loss with a few remaining posterior teeth.**Lower Left Region (Quadrant 3)**- **Number of Teeth:** 4 teeth are visible. This quadrant contains some posterior teeth, and there is evidence of significant dental restoration or prosthetics, including what appears to be a partial denture or bridge.**Lower Right Region (Quadrant 4)**- **Number of Teeth:** 3 teeth are present. Similar to the other quadrants, there is extensive tooth loss with only a few teeth remaining, which are also restored or part of a prosthetic device.**Overall Assessment**:**

- This dental X-ray indicates severe tooth loss in all quadrants with extensive use of dental prosthetics and restorations. The teeth that are present are mostly posterior (back) teeth, and most of the visible dental structures are part of restorative or replacement solutions such as bridges or partial dentures.

The condition of the gums and the bone structure would need thorough clinical evaluation to ensure the continued suitability of the existing dental prosthetics and to consider any additional restorative work or replacements needed to maintain functional mastication and aesthetics. Regular follow-ups and potentially further restorative treatments might be necessary to maintain oral health and function.

Claude-3-Opus

Based on the dental X-ray provided, I will conduct a professional assessment of the teeth present, dividing them into the four requested regions:

Upper right region:

- 8 teeth present: central incisor, lateral incisor, canine, 1st and 2nd premolars, 1st, 2nd and 3rd molars

Upper left region:

- 8 teeth present: central incisor, lateral incisor, canine, 1st and 2nd premolars, 1st, 2nd and 3rd molars

Lower left region:

- 8 teeth present: central incisor, lateral incisor, canine, 1st and 2nd premolars, 1st, 2nd and 3rd molars

Lower right region:

- 8 teeth present: central incisor, lateral incisor, canine, 1st and 2nd premolars, 1st, 2nd and 3rd molars

In total, all 32 teeth are present in the X-ray. There are no visible defects or missing teeth in any of the regions based on the provided image.

GPT-4o

Based on the panoramic dental X-ray provided:****Upper Right Region:**- Contains 5 teeth, with significant dental restorations (crowns).**Upper Left Region:**- Contains 7 teeth, with several dental restorations (crowns) and one impacted third molar.**Lower Left Region:**- Contains 5 teeth, with one tooth being significantly restored and an absence of third molars.**Lower Right Region:**- Contains 6 teeth, with several teeth restored with crowns and absence of third molar. There are multiple dental restorations noted, particularly crowns, in the upper and lower regions. Additionally, there are signs of missing and impacted teeth.** No significant pathology noted in the provided image.

Figure 26: **Dental Image: Case 4.** The task involves quantifying the number of teeth and identifying anomalies in dental X-rays, with critical information highlighted in yellow.